Chapter 1:

Introduction

1.1 Background and Motivation

The idea of nanotechnology was proposed by Richard Feynman during his talk 'There is plenty of room at the bottom' in 1959 where he envisioned a world in which individual atoms and molecules can be manipulated, though the term nanotechnology was coined later on. Nanotechnology has enabled the development of novel advanced nanomaterials with potential application in almost every field. These nanomaterials have at least one dimension in the range of 1-100nm. Of importance are semiconductor nanomaterials that exhibit unique size-dependent electrical, mechanical, chemical and optical properties which are largely due to the quantum size effects and large surface to volume ratio. Reducing the size of a material from bulk to nanoscale causes its physical and chemical properties to completely change allowing unique size-dependent properties to manifest [1]. The nanomaterials have different shapes and morphologies which range from 0D, 1D and 2D. Zero dimensional (0D) nanomaterials include nanoparticles which can be in different shapes like spherical, cubic, diamond etc, whereas one dimensional (1D) nanomaterials namely nanowires, nanorods, nanotubes have varying lengths and diameters (different aspect ratios) and two-dimensional (2D) nanomaterials are generally thin film materials.

Zinc oxide (ZnO) nanomaterial is one of the most important nanomaterials for nanotechnology in today's research [2]. There are a great vast of opportunities presented by zinc oxide nanomaterial and is also attractive because of its non-toxicity and can easily be produced using simpler processes and low-cost technologies at low temperatures. By altering the growth conditions, different nanostructures and properties of zinc oxide nanomaterial can be realized.

1.2 ZnO Crystal Structure

ZnO is a semiconductor material with a direct wide band gap energy of 3.37 eV and a large exciton binding energy 60 meV at room temperature [3]. ZnO nanomaterial exhibits dual emission at room temperature. The first one is near-band edge emission due to the exciton radiative recombination and the other one is visible emission which is due to defect energy states such as oxygen vacancies. ZnO crystallizes in three forms which are hexagonal wurtzite, cubic zinc blende and the cubic rock salt structure as shown in fig 1.1 below. Under general conditions, ZnO exhibits a hexagonal wurtzite structure. The crystalline nature of ZnO could be indexed to known structures of hexagonal ZnO, with nm, nm, and nm (JCPS card no. 36–1451) [4]. The ratio of of about 1.60 is close to the ideal value for a hexagonal cell [5]. The zinc blende structure can be stabilized only by growth on cubic substrates, and the rock salt structure may be obtained at relatively high pressures.

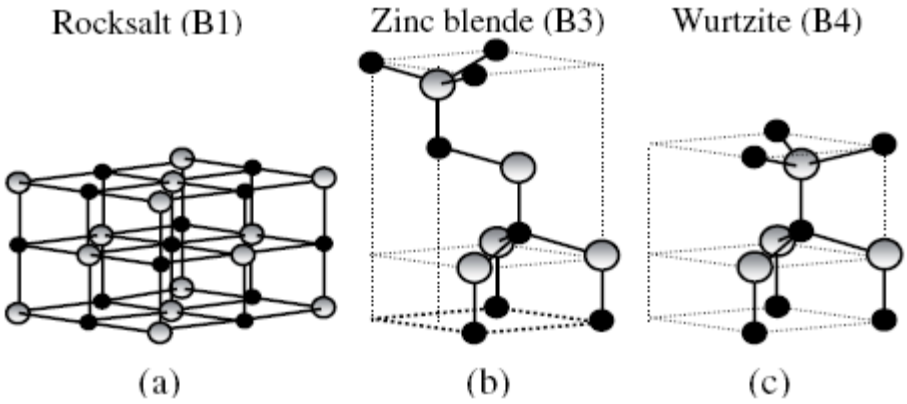

Fig 1.1. ZnO crystal structures: (a) cubic rock salt (B1), (b) cubic zinc blende (B3), and (c) hexagonal wurtzite (B4). Shaded gray and black spheres denote Zn and O atoms, respectively.

1.3 Physical Parameters

Some important properties of ZnO nanoparticles are given below:

Table 1.1 Physical Parameters

Parameter	**Value**
Stable Phase at 300K	Wurtzite
Lattice Parameters	'a' = 3.2495 Å 'c' = 5.2069 Å
Density	5.606 g/cm^3
Melting point	1975ºC
Static dielectric constant	8.656
Refractive index	For wurtzite – 2.049 For zinc blende – 2.008
Energy gap	3.37 eV, direct
Exciton Binding energy	60 meV
Electron effective mass	0.24
Hole effective mass	0.59

1.4 Electronic band structure

Knowledge of the band structure is critical for device applications. Different methods have been used to measure the electronic core levels in solids and these include X-ray or UV reflection/absorption or emission techniques, photoelectron spectroscopy (PES) and angle-resolved photoelectron spectroscopy (ARPES).

ZnO is a direct band gap semiconductor with the uppermost valence and the lowest conduction bands (VB and CB, respectively) at the same point in the Brillouin zone, the Γ-point (k = 0).

A typical representation of the band structure looks as follows [6]:

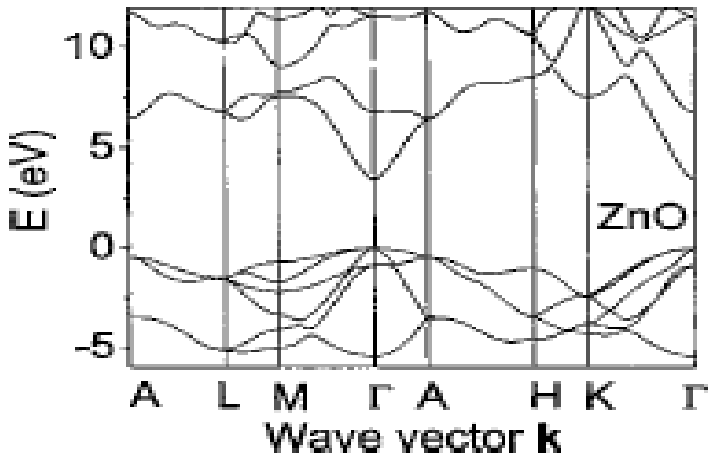

Fig 1.2: Band Diagram

1.5 Review on the synthesis of ZnO nanomaterials

Bertrand Faure et al [7] described the principles of deagglomeration for oxide nanoparticles including zinc oxide nanoparticles and their stabilization in both aqueous and non-aqueous media. They mentioned that oxide nanoparticles heavily agglomerated can severely limit the utilization of the inherent properties, pose substantial processing challenges and complicate the dispersion and functionalization of the nanoparticles and that the films and coatings produced from aggregated gas-phase powders are often hazy, with poor adhesion to the substrate. They also stated that agglomeration is commonly observed in nanopowders that have been produced in the gas phase or dried from the liquid phase, as shown for titania in figure 1.3 below

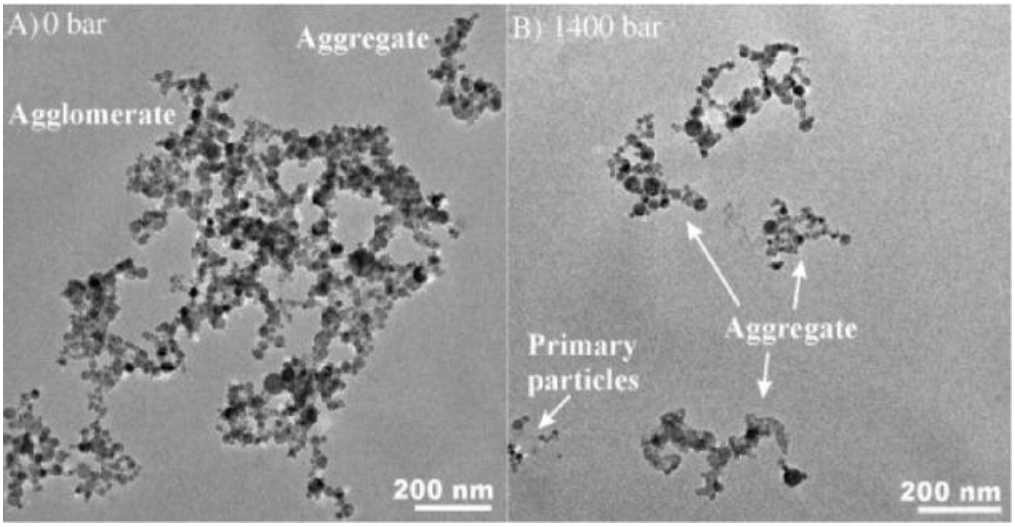

Figure 1.3: The effect of high-pressure deagglomeration on the morphology and size of the aggregates of flame-made TiO_2 particles [7]

Milling, high-shear mixing and ultrasonication are commonly used to break down agglomerates [7] and in this project work a post thermal treatment was employed. Concentrated zinc oxide nanocrystal suspensions can be obtained by adding a base (LiOH, NaOH or tetramethylammonium hydroxide) to zinc acetate dihydrate dissolved in alcohol [8–10]. The acetate-capped nanoparticles obtained by this sol–gel method exhibit photoluminescence both in the near UV (370 nm) and in the visible range (500–550 nm), the former being related to excitonic emission and the latter to the presence of oxygen

vacancies on the surface. The visible emission might be problematic for some applications and can be quenched by a thermal post-treatment or copper doping [11][7]. **Haibo Zeng et al** [12] synthesized ZnO nanoparticles that exhibit very strong blue emissions, the intensity of which first increase and then decrease with annealing and also concluded that high concentrations of defects are introduced into nanoscale ZnO through non-equilibrium processes. **S.K.Patra** [13] fabricated ZnO nanorods by preparing an alkali solution of zinc by dissolving 14.87g of zinc nitrate and 4g of NaOH in distilled water to form a 100ml solution. Then the NaOH solution was heated to approx. 40°C. Under constant stirring, the zinc nitrate solution was added slowly (dropwise for 30min) to the above alkali solution. ZnO nanorods were of diameter ~20nm and length ~ (100-150) nm.

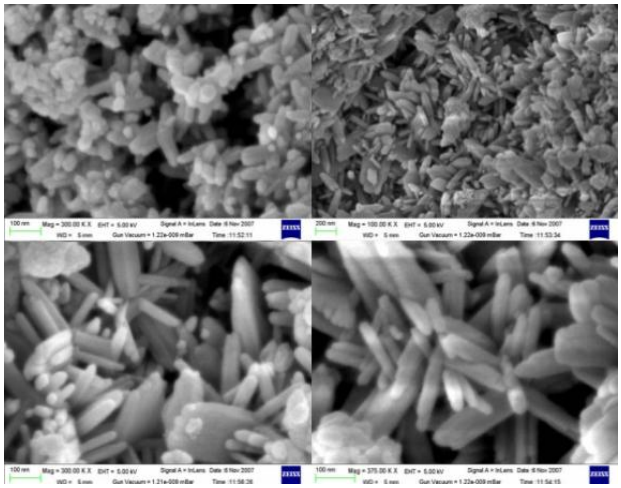

Fig 1.4: FESEM diagram of the synthesized nanorods by S.K. Patra [13]

Chittaranjan Bhakat et al [14] synthesized uniform ZnO nanorods with diameters of 100-200nm and lengths of about 1µm. Solution of zinc acetate dehydrate was prepared by dissolving 2.195g of zinc acetate dehydrate in 100ml distilled water/ethanol and stirred in ambient atmosphere. KOH 1.122g is dissolved in 10ml distilled water and was added to the above solution dropwise under continuous stirring. The mixture was then further heated for 3hr at 80-90°C without stirring. **Li-Li Han et al** [15] synthesized ZnO quantum dots (QDs) with blue emission by a sol–gel method. They discovered that the blue emission arises from neither the quantum confinement nor intermediate products,

and it can be achieved only in the presence of Li^+ cations and excessive OH^- anions. The blue emission was also determined as the electron transition from the conduction band to interstitial oxygen defects. Excessive OH^- anions are responsible for the formation of interstitial oxygen defects, and Li^+ ions can stabilize the defects by substituting for Zn atoms. **Sumetha Suwanboon et al** [16] successfully synthesized one-dimensional ZnO nanoparticles from $Zn(CH_3COO)_2.2H_2O$ as well as CTAB-assisted HMTA solutions. The entire calcined ZnO nanoparticles indexed with the hexagonal wurtzite structure. Columnar hexagonal-like ZnO structures were shaped when aqueous HMTA solution was used as the precipitating agent. They stated that the growth rate along the (0001) plane of ZnO nuclei is very much slower than that of the branch rod-like formation and that the six side facets of the (1010) family could promote their growth , resulting in the formation of columnar hexagonal-like structure.

Table 1.2. Information of the synthetic conditions and ZnO particles obtained [16]

Precipitating Agent	CTAB Concentration (mol)	Crystallite Size (nm)	Particle size (diameter) (nm)	Particle Shape
HMTA	0	49.48	501	Columnar Hexagonal
	0.01	47.17	473	
	0.02	45.41	436	
NaOH	0	46.81	274	Branch Rod
	0.01	42.85	202	
	0.02	41.26	148	

S. Chakraborty et al [17] successfully synthesized flower-like ZnO nanostructures by the simple chemical precipitation method at room temperature in distilled water medium and without using any capping agent. The UV–visible optical absorption measurement shows the presence of UV absorption at ~260 nm in the sample dispersed in water. The room-temperature PL spectrum of the sample consists of near-band edge emission at ~360 nm as well as a violet emission band at 420nm

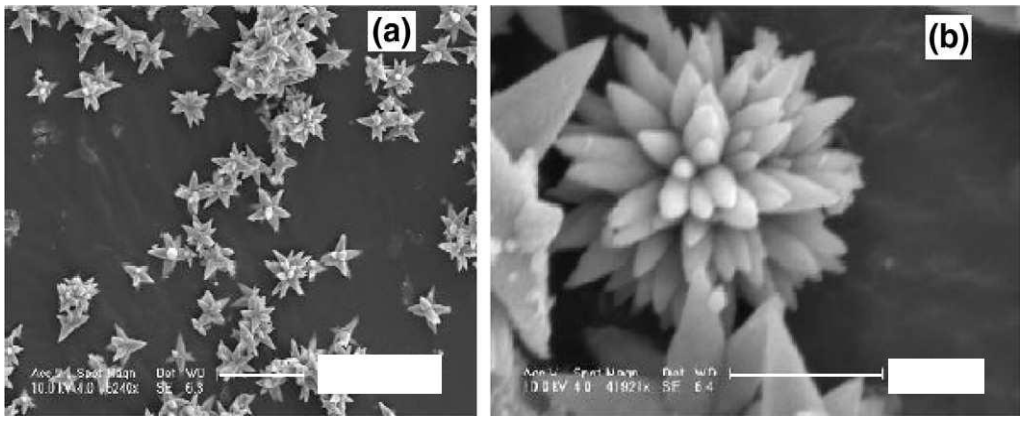

Fig 1.5: Scanning electron microscope (SEM) images of the ZnO nanoflowers are shown in (a) and a magnified image is shown in (b) [17]

Xinyu Zhang et al [18] synthesized ZnO nanorods based on the modified method by Lin et al [19] with mechanical assisted. They found that an increase in the calcination temperature led to an increase in the average particle sizes. ZnO nanorods calcined at 350°C had a length of about 800 nm, and diameter is about 30–50 nm. When the temperature was raised to 400°C and 450°C, there is increase in diameter and decrease in length of the nanorods and further rise in temperature to 500°C produces irregular particles (average size ~100 nm). They concluded that as the calcination temperature increases, the particle morphology changes from rod to irregular shape. The band gap energy (E_{bg}) of ZnO was calculated from the following equation, $E_{bg} = 1240/\lambda$ (eV) [20][21][22], where E_{bg} is the bandgap energy in eV and λ is the wavelength in nanometers.

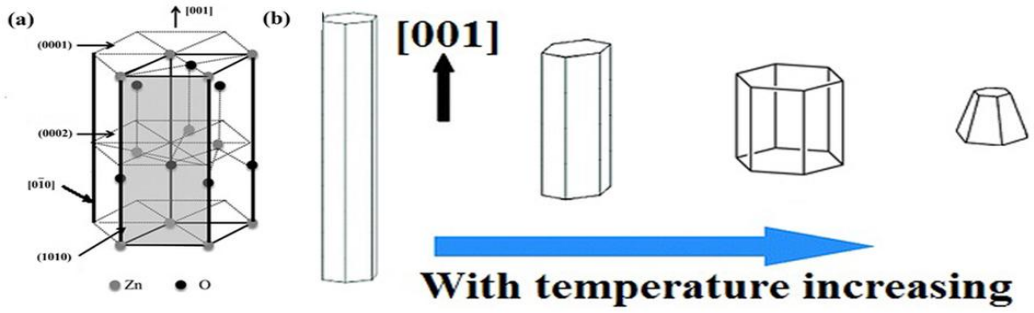

Fig 1.6: (a) Shape of the nanorod. Note, [uvw] is an index of a specified crystal axis and (hkil) is an index of a specified crystal plane. (b) Schematics of nanorods growth with increasing temperature [18]

Hui Zhang et al [23] fabricated ZnO nanowires by a simple chemical sol–gel process. The ZnO nanowires have a hexagonal structure and the diameters are very uniform, at about 60 nm. **Hongxia Zhang et al** [24] prepared ZnO nanorods through wet chemical method by using zinc nitrate hexahydrate and ammonium hydroxide in the presence of PEG. The ZnO nanorods have a wurtzite structure and the PL spectra produced blue emission at 466 nm and green–yellow emission at 542 nm. **Rizwan Wahab et al** [25] employed low temperature solution synthesis to make flower-shaped ZnO nanostructures which composed of hexagonal ZnO nanorods. Room- temperature photoluminescence (PL) demonstrated a strong and dominated peak at 381 nm with a suppressed and broad green emission at 515 nm. **Changle Wu et al** [26] employed a novel chemical route to prepare ZnO nanoparticles. Their results revealed that with the increase of the reaction temperature, the morphology of particles seems to change from rod-like to short prism-like form. The photoluminescence band was at near 380 nm and no other bands were observable, which proved to exhibit high optical property and might have potential application in nanoscale optoelectronic devices.

1.6 Applications

ZnO nanostructures have potential use in different fields due to their unique physical and chemical properties.

Gas Sensing

Different gases that have been detected by ZnO nanostructures include ammonia, nitrogen oxide, hydrogen and oxygen. ZnO nanostructures have a large surface area which allow them to be more sensitive to the adsorption or desorption of gas molecules on their surface [27].

Biosensing

Non-toxicity, bio-compatibility and high electron transfer rates are some of the interesting properties of ZnO nanostructures which make them favorable for the detection of biological entities [28].

UV Detection

ZnO nanostructures have been applied for UV photodetection by various research groups [29].

UV Lasers

Growth conditions of ZnO nanostructures can be manipulated so as to eliminate defects-related emissions allowing them to be applied for UV laser applications [30].

Light-Emitting Diodes

Research groups like *Harnack et al* [31] have demonstrated that the electrical characteristics of ZnO nanorods show diode-like behavior allowing them potential use in LEDs

Solar Cells

The large surface area and high electron transfer rates of ZnO nanostructures make them potential candidates as electrodes in dye-sensitized solar cells (DSSCs [32].

Field Emission Devices

ZnO nanostructures particularly with sharp tips have shown good field emission characteristics making them applicable as electron emitting sources [33].

Field Effect Transistors

The ZnO nanostructure acts as the channel which controls the current flow from the drain to the source through manipulation of the gate voltage [34].

Photocatalysis

ZnO nanostructures have a large surface area and surface properties favorable for photocatalysis [35].

1.7 Aims and Objectives

The aim of this project work was on the following steps:

- Synthesis of zinc oxide nanoparticles and nanorods by the sol-gel method
- Study on the effect of temperature on the morphology of the nanostructures
- Effect of surfactants ethylene glycol (EG) and ethylenediamine (EDA) on the morphology of the nanostructures
- Characterization of the surface morphology using SEM
- Determination of the chemical composition using EDX
- Study of the optical properties by UV/Vis and PL spectroscopy
- Characterization of the crystal structure and investigate the particle size using XRD

Chapter 2:

Experimental and Characterization Techniques

2.1 The Sol-Gel process

Sol-gel refers to a process in which solid nanoparticles dispersed in a liquid (a sol) agglomerate together to form a continuous three-dimensional network extending throughout the liquid (a gel). The chemical reactions that occur during a sol-gel process are hydrolysis, poly-condensation, and gelation. During hydrolysis and poly-condensation, a colloid (sol), which consists in nanoparticles dispersed in a solvent, is formed. The existing sol phase transforms to the gel. The resulting gel-phase is formed by particles which size and formation can vary greatly from discrete colloidal particles to continuous chain-like polymers.

The sol-gel process is a less expensive, simple versatile solution process for making advanced materials in a wide variety of forms: ultrafine or uniform powders, thin film coatings, fibers, porous or dense materials, and extremely porous aerogel materials. An overview of various sol-gel processes is illustrated below in fig 2.2

Sol-gel includes the following steps:

1. Making sol or precipitating powder, gelling the sol in a mold or on a substrate (in case of films), or making a second sol from the precipitated powder and its gelation, or shaping the powder into a body by non-gel routes;
2. Drying;
3. Firing and Sintering. [Rabinovich 1994]

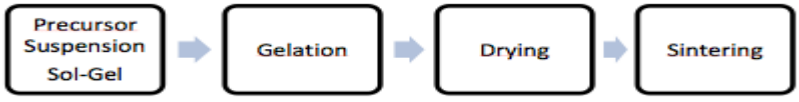

Fig 2.1: Simplified downstream processes

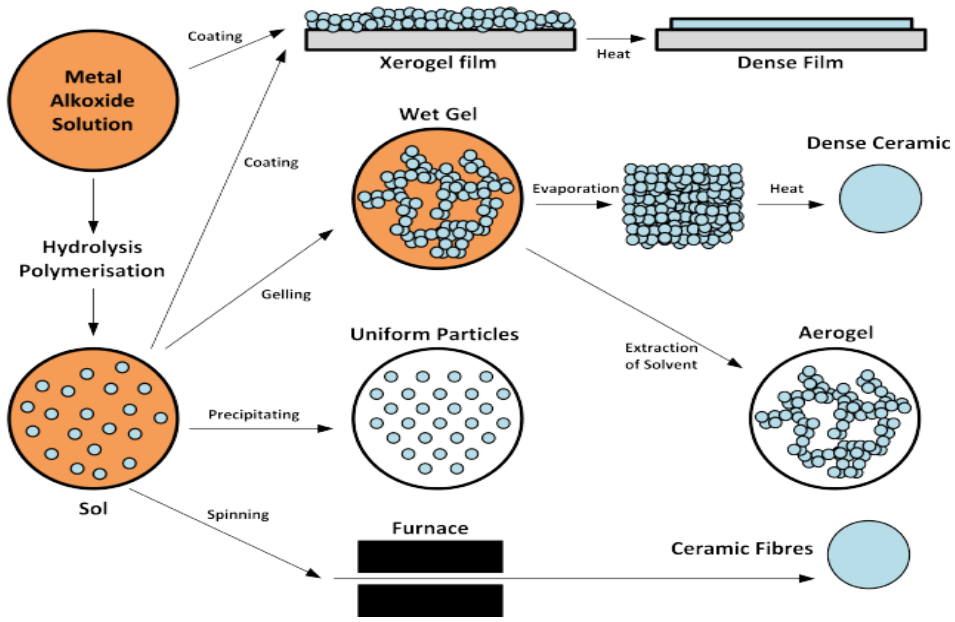

Fig 2.2: Schematic representation of the different stages and routes of the sol-gel technology.

Factors that affect Sol-Gel Chemistry

Sol-gel chemistry tends to be particularly sensitive to the following parameters:

Solvent. As molecules assemble together (polymerize) into nanoparticles, the solvent needs to be able to keep the nanoparticles dissolved so that they don't precipitate out of the liquid. Also, the solvent can play a role in helping nanoparticles connect together. As a result, the solvent makes a big difference in ensuring a gel network can form.

Temperature. The chemical kinetics of the different reactions involved in the formation of nanoparticles and the assembly of nanoparticles into a gel network are accelerated by temperature, meaning the gel time is affected by temperature. If the temperature is too low, gelation may take weeks or months. If the temperature is too high, the reactions that join nanoparticles together into the gel network occurs so quickly that clumps form instead and solid precipitates out of the liquid.

- **Reaction-generated heat** released from chemical reactions involved in the formation of nanoparticles and gel networks can feed back into the solution and

cause things to react faster, releasing even more heat, causing things to react even faster, etc.

Time. Depending on the type of gel being made, different steps in the gel formation process work differently over different time scales. In general, slower is better for sol-gel. If a gel is allowed to form slowly, it usually has a much more uniform structure. Speeding reactions up too much causes precipitates to form instead of gel network, and can make a gel cloudy and weak or simply not form.

Catalysts. A catalyst is a chemical that accelerates a chemical reaction but does not get used up in doing so. In a lot of sol-gel chemistry, both acids (H^+) and bases (OH^-) are catalysts, but accelerate chemical reactions by different mechanisms. This is another reason why sol-gel chemistry is usually pH sensitive. Small amounts of catalysts ("catalytic amounts"), on the order of milligrams per tens of milliliters of solution can cause drastic changes in gel time–in many cases reducing gel time from hours, days, or weeks to minutes.

pH. Any colloidal chemistry that involves water is sensitive to pH.

Agitation. Mixing a sol as it gels is important to ensure that the chemical reactions in the solution occur uniformly and that all molecules receive an adequate supply of chemicals they need for the reactions to proceed properly. However, as a sol gels, there are microscopic and macroscopic domains of partially-formed gel network throughout the liquid, and agitation can sometimes disrupt the formation of these domains, meaning they get broken up, however usually the broken network fragments regrow and a solution-wide network results.

2.2 Characterization Techniques

To investigate structure, surface morphology, topography, chemical composition, absorbance, emission of synthesized ZnO nanomaterials, the following techniques were used:

2.2.1 Structural and Morphological Characterization

- X-Ray Diffraction (XRD)
- Scanning Electron Microscope (SEM)

2.2.2 Optical Characterization

- UV-Vis spectroscopy
- Photoluminescence spectroscopy

2.2.1.1 X-Ray Diffraction (XRD)

X-rays are electromagnetic radiation with wavelengths between about 0.02Å and 100Å. They have wavelengths similar to the size of atoms and can penetrate matter more easily.

X-ray diffraction (XRD) is a fast, non-destructive technique that can be applied to single crystal, polycrystalline and amorphous materials and provides information such as the structure of crystalline materials, electron distribution within the atoms and throughout the unitcell, orientation of single crystals, texture of polygrained materials, crystalline phases, defects and can differentiate between crystalline and amorphous materials.

X-ray diffraction measurement

A crystal mounted on a sample holder is rotated while being exposed to x-rays, producing a diffraction pattern. The specimen atoms' electrons scatter x-ray waves which interfer constructively in certain directions according to Bragg's law:

$$n\lambda = 2d\sin\Theta$$

where d-spacing between diffracting planes, Θ- incident angle, n- integer usually 1, λ- beam wavelength. The X-Ray diffraction process in accordance with Bragg's law is shown below in fig 2.3

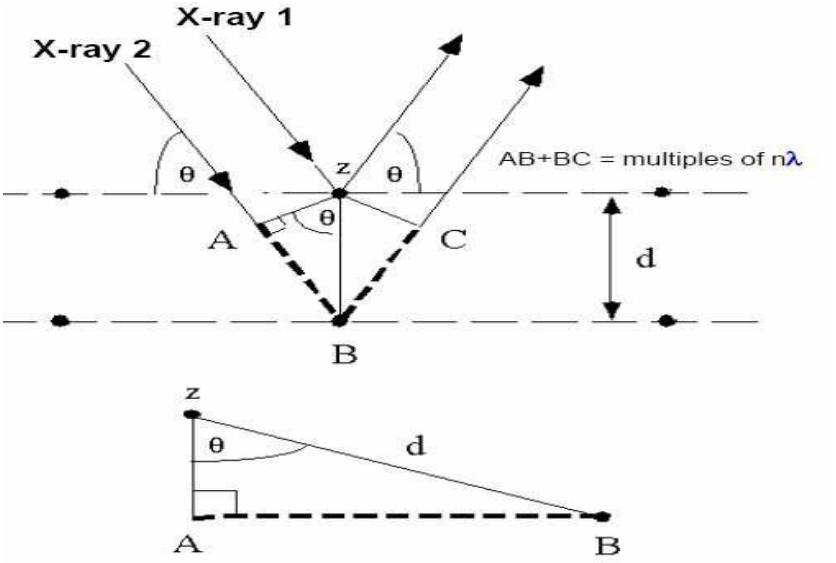

Figure 2.3: X-ray Diffraction in accordance with Bragg's Law

Crystallite size determination

The grain size is estimated using the Scherrer equation:

$$d = \frac{B\lambda}{\beta \cos\theta}$$

Where λ- wavelength of x-rays, Θ- diffraction angle, B- usually 0.9, β– full width at half maximum (FWHM)

Fig 2.4: Bruker D8 ADVANCE X-Ray Diffractometer at DTU

Description of X-Ray Diffractometer (Bruker D8 ADVANCE)

The Bruker D8 Advance is a Cu-source, theta-theta diffractometer equipped with a Lynx-eye position sensitive detector. This detector allows for a range of scattering angles to be measured simultaneously, increasing signal detection and decreasing scan times. Two sample stages are installed with the diffractometer: 1) A rotation stage for increased crystallite illumination and 2) an Anton-Paar CHC Cryo & Humidity stage. Samples can be heated or cooled under and inert atmosphere or vacuum from - 190°C to 300°C, allowing for temperature dependent phase identification. The sample stage is also equipped to handle various level of humidity for biological applications. The Bruker D8 Advance is ideal for temperature dependent x-ray diffraction analysis of inorganics, pharmaceutics, and organic systems which require precise temperature control [45]

2.2.1.2 Scanning Electron Microscope (SEM)

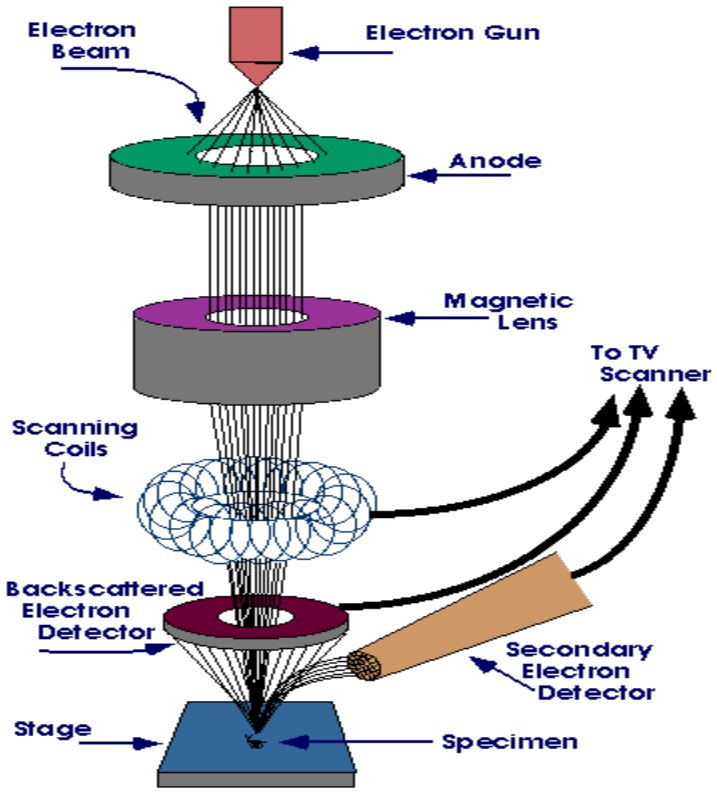

Fig 2.5: Schematic diagram of the SEM [36]

The scanning electron microscope (SEM) obtains information such as surface topography, morphology, surface fractures and chemical composition.

As shown in fig 2.5 above, the SEM uses a focused beam of high energy electrons produced by an electron gun instead of light allowing high resolution. The electron beam travels in a vacuum from the electron gun and is focused to the sample by means of electromagnetic fields and lenses and upon striking the sample surface electrons and x-rays are ejected [37].

The different types of particles emitted are shown below in fig 2.6

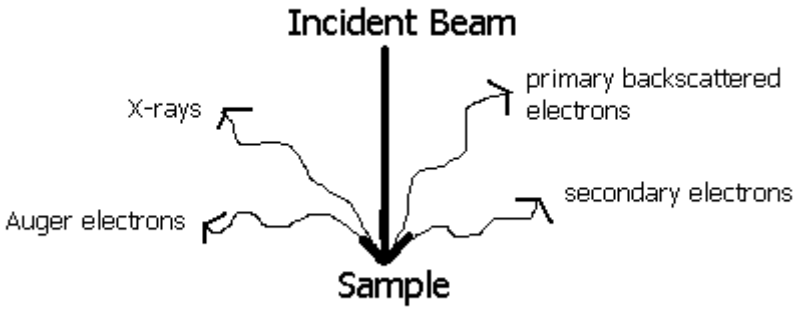

Fig 2.6: Different types of particles emitted

The X-rays, backscattered electrons (BSE) and secondary electrons are then collected by the detectors to provide information about the sample.

The secondary electrons are low energy electrons which originate from near the sample surface and therefore provide information about the surface topography and the BSE are high energy electrons that are reflected back through interaction with the specimen atoms and as such are used to detect contrast between areas with different chemical compositions [38].

The X-rays produced may also provide information for elemental analysis in EDX spectroscopy but however is not reliable as it is usually associated with false peaks, noise from amplifiers and microphonics [39].

Fig 2.7: HITACHI S-3700N SEM at DTU

Description of SEM (Hitachi S-3700N)

The Hitachi S-3700N SEM is a conventional microscope with tungsten electron source which features a high vacuum observation method which does not permit observation of non-conductive samples such as electronic components, and water containing samples such as cultured cells, without any sample preparation. Sample preparation is done by coating them with a thin layer of gold using an ion sputtering machine before inserting them into the SEM [37]. The SEM also has accessories such as EDX for elemental composition analysis. The SEM requires a vibration free environment and is designed for high-voltage operation with accelerating voltages of up to 15kV.

2.2.2.1 UV/Vis spectroscopy

Principle of UV-Vis absorption

Absorption measures transitions from the ground state to the excited state [40]. Molecules containing π-electrons or non-bonding electrons (n-electrons) can absorb the energy in the form of ultraviolet or visible light to excite these electrons to higher anti-bonding molecular orbitals [41]. The more easily excited the electrons (i.e. lower energy gap between the HOMO and the LUMO), the longer the wavelength of light it can absorb.

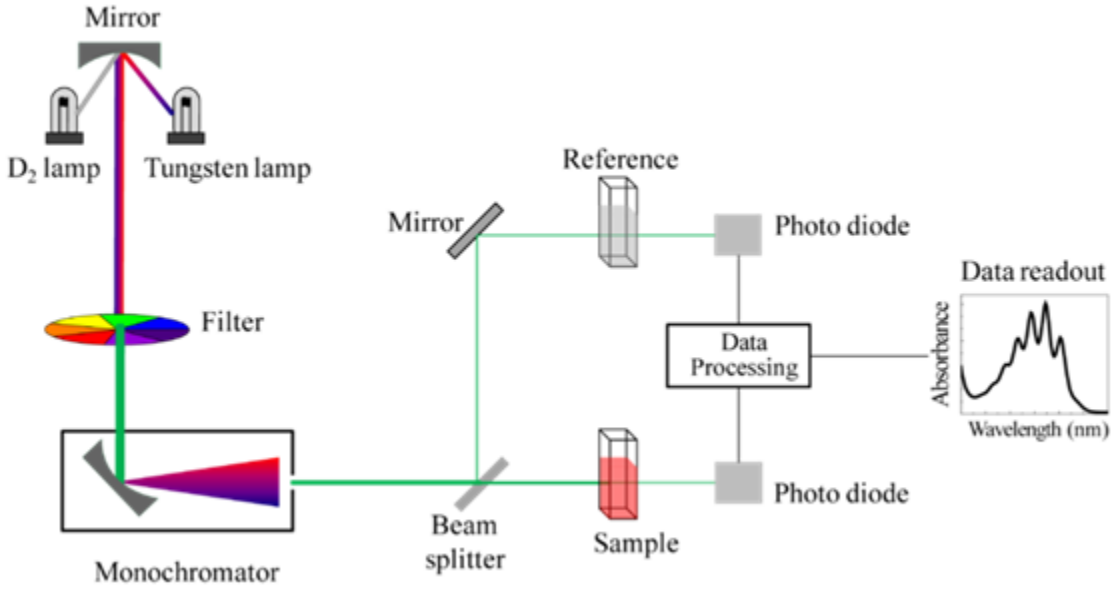

Fig 2.8: Schematic diagram of the UV/Vis spectrophotometer

The UV/Vis spectrophotometer measures the intensity of light passing through a sample (I), and compares it to the intensity of light before it passes through the sample (I_o). The ratio I/I_o is called the *transmittance*, and is usually expressed as a percentage (%T). The absorbance, A, is based on the transmittance:

$$A = -\log(\%T/100\%)$$

A spectrometer records the degree of absorption by a sample at different wavelengths and the resulting plot of absorbance (A) versus wavelength (λ) is known as a spectrum. The wavelength at which the sample absorbs the maximum amount of light is known as λ_{max}

As shown in fig 2.8 above, the light is split into two beams before it reaches the sample. One beam is used as the reference; the other beam passes through the sample. The reference beam intensity is taken as 100% Transmission (or 0 Absorbance), and the measurement displayed is the ratio of the two beam intensities. Some double-beam instruments have two detectors (photodiodes), and the sample and reference beam are measured at the same time. In other instruments, the two beams pass through a beam chopper, which blocks one beam at a time. The detector alternates between measuring the sample beam and the reference beam in synchronism with the chopper.

The **Beer-Lambert law** states that the absorbance of a solution is directly proportional to the concentration of the absorbing species in the solution and the path length [42]. UV/Vis is most often used in a quantitative way to determine concentrations of an absorbing species in solution, using the Beer-Lambert law:

$$A = \log_{10}(I_0/I) = \epsilon c L,$$

where *A* is the measured absorbance, in **A**bsorbance **U**nits (**AU**), I_0 is the intensity of the incident light at a given wavelength, I is the transmitted intensity, *L* the path length through the sample, and *c* the concentration of the absorbing species. For each species and wavelength, ε is a constant known as the molar absorptivity or extinction coefficient. This constant is a fundamental molecular property in a given solvent, at a particular temperature and pressure [43].

Applications

UV/Vis spectroscopy is routinely used in analytical chemistry for the quantitative determination of different analytes, such as transition metal ions, highly conjugated

organic compounds, and biological macromolecules. Specially to understand the interaction of radiation with the matter.

The wavelengths, FWHM and shape of absorption can be correlated with the types of transitions and corresponding energy, which are valuable in determining the structure of the molecules and nanomaterials.

Fig 2.9: PerkinElmer Lambda 750 UV/Vis/NIR Spectrophotometer at DTU

Description of Spectrophotometer (PerkinElmer Lambda 750 UV/Vis/NIR)

The Lambda 750 UV/Vis/NIR spectrophotometer is designed to provide the maximum sampling flexibility for tough samples in chemistry, biochemistry and materials science. Turbid and cloudy liquids and suspensions are handled with ease by the Lambda 750, which can make highly accurate measurements up to 6 absorbance units. It uses the twin deuterium and tungsten-halogen source lamps. True double beam, double monochromator design provides the highest possible stability coupled with the highest

accuracy and lowest stray-light performance. The Lambda 750 measures wavelengths in the range of 190nm – 3300nm with a UV/Vis resolution of 0.17 – 5.00nm.

2.2.2.2 Photoluminescence (PL) spectroscopy

Photoluminescence spectroscopy is a contactless, nondestructive method of probing the electronic structure of materials. Light is directed onto a sample as shown in fig 2.10 below, where it is absorbed and imparts excess energy into the material in a process called photo-excitation. One way this excess energy can be dissipated by the sample is through the emission of light, or luminescence. In the case of photo-excitation, this luminescence is called photoluminescence.

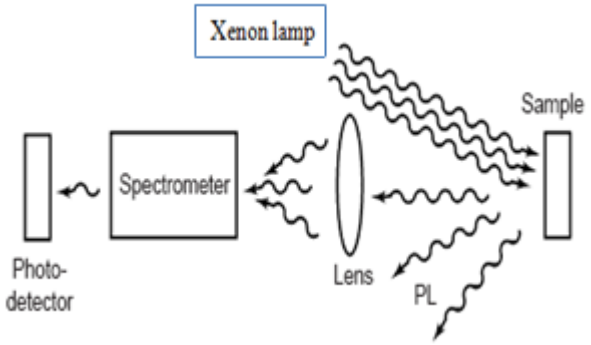

Figure 2.10: Typical experimental set-up for PL measurements.

Photo-excitation causes electrons within a material to move into permissible excited states. When these electrons return to their equilibrium states, the excess energy is released and may include the emission of light (a radiative process) or may not (a non-radiative process). The energy of the emitted light (photoluminescence) relates to the difference in energy levels between the two electron states involved in the transition between the excited state and the equilibrium state. The quantity of the emitted light is related to the relative contribution of the radiative process.

Photoluminescence spectroscopy provides a good method for the study of luminescent properties of a fluorophore, bandgap determination, impurity levels and defect detection, recombination mechanisms, surface structure and excited states [44].

Fig 2.11: HORIBA Jobin Yvon Fluorolog 3 (FL3-22) Spectrofluorometer at DTU

Description of Spectrofluorometer (HORIBA Jobin Yvon Fluorolog 3)

The fluorolog 3 spectrofluorometer uses a 450W xenon excitation lamp mounted vertically to image the arc on the slit for more throughput. It has a standard detector (photomultiplier tube) that covers the full range from UV to near-IR with a resolution of 0.2nm and an accuracy of ±0.5nm. The fluorolog 3 is the ultimate in stray-light rejection, and the double-grating monochromators in excitation and emission positions are perfect for highly scattering biological samples like lipids and proteins, or solids like powders, semiconductors or phosphors.

References

[1] Nel A, Xia T, Madler L, Li N. Toxic potential of materials at the nanolevel. Science. 2006:**311**:622-7

[2] Z. L. Wang, "Ten years' venturing in ZnO nanostructures: from discovery to scientific understanding and to technology applications," Chinese Science Bulletin, vol. **54**, no. 22, pp. 4021–4034, 2009

[3] F. Lu, W. Cai, and Y. Zhang, "ZnO hierarchical micro/nanoarchitectures: solvothermal synthesis and structurally enhanced photocatalytic performance," Advanced Functional Materials, vol. **18**, no. 7, pp. 1047–1056, 2008.

[4] M. Mehrabian, R. Azimirad, K. Mirabbaszadeh, H. Afarideh, and M. Davoudian, "UV detecting properties of hydrothermal synthesized ZnO nanorods," Physica E, vol. **43**, no. 6, pp. 1141–1145, 2011.

[5] C. F. Klingshirn, "ZnO: material, physics and applications," ChemPhysChem, vol. **8**, no. 6, pp. 782–803, 2007.

[6] W.J. Fan, J.B. Xia, P.A. Agus, S.T. Tan, S.F. Yu and X.W. Sun
Journal of Applied Physics **99**, 013702 (2006)

[7] Bertrand Faure, German Salazar-Alvarez, Anwar Ahniyaz, Irune Villaluenga, Gemma Berriozabal, Yolanda R De Miguel and Lennart Bergström 2013 *Sci. Technol. Adv. Mater.* **14** 023001

[8] Spanhel L and Anderson M A 1991 J. Am. Chem. Soc. **113** 2826

[9] Meulenkamp E A 1998 J. Phys. Chem. B **102** 5566

[10] Wood A, Giersig M, Hilgendorff M, Vilas-Campos A, Liz-Marzan L M and Mulvaney P 2003 Aust. J. Chem. **56** 1051

[11] Spanhel L 2006 J. Sol–Gel Sci. Technol. **39** 7

[12] Haibo Zeng, Guotao Duan, Yue Li, Shikuan Yang, Xiaoxia Xu and Weiping Cai (February 2010) Advanced Functional Materials **20** No 4 561–572

[13] A novel chemical approach to fabricate ZnO nanostructures by Saroj Kumar Patra (*thesis*)

[14] Chittaranjan Bhakat, Prasoon Pal Singh. jul-aug.2012 International Journal of Modern Engineering Research (IJMER) **2** No 4 pp-2452-2454

[15] Li-Li Han, Lan Cui, Wei-Hua Wang, Jiang-Long Wang and Xi-Wen Du 2012 *Semicond. Sci. Technol.* **27** 065020

[16] Sumetha Suwanboon, Pongston Amornpitoksuk and Supasarote Muensit Journal of Ceramic Processing Research, Vol. **11**, No. 4, pp. 419-424 (2010) Enhancement of optical bandgap and luminescent characteristics of one-dimensional ZnO nanoparticles

[17] S. Chakraborty, A.K. Kole, P. Kumbhakar Room temperature chemical synthesis of flower-like ZnO nanostructures, Materials Letters **67** (2012) 362–364

[18] Effect of aspect ratio and surface defects on the photocatalytic activity of ZnO nanorods Xinyu Zhang, Jiaqian Qin, Yanan Xue, Pengfei Yu, Bing Zhang, Limin Wang, Riping Liu Scientific Reports **4**, Article number: 4596

[19] Lin, C.-C. & Li, Y.-Y. Synthesis of ZnO nanowires by thermal decomposition of zinc acetate dihydrate. Mater. Chem. Phys. **113**, 334–337 (2009).

[20] Bhatkhande, D. S., Pangarkar, V. G. & Beenackers, A. A. C. M. Photocatalytic degradation for environmental applications – a review. J. Chem. Technol. Biotechnol. **77**, 102–116 (2002).

[21] Orel, Z. C., Gunde, M. K. & Orel, B. Application of the Kubelka-Munk theory for the determination of the optical properties of solar absorbing paints. Prog. Org. Coat. **30**, 59–66 (1997).

[22] Madhusudan Reddy, K., Manorama, S. V. & Ramachandra Reddy, A. Bandgap studies on anatase titanium dioxide nanoparticles. Mater. Chem. Phys. **78**, 239–245 (2003).

[23] Hui Zhang, Xiangyang Ma, Jin Xu, Junjie Niu and Deren Yang, Nanotechnology **14** (2003) 423–426

[24] Hongxia Zhang, Jing Feng, Jun Wang, Minlin Zhang , Materials Letters **61** (2007) 5202–5205

[25] Rizwan Wahab, S.G. Ansari, Y.S. Kim, H.K. Seo, G.S. Kim, Gilson Khang, Hyung-Shik Shin, Materials Research Bulletin **42** (2007) 1640–1648

[26] Changle Wu, Xueliang Qiao, Jianguo Chen, Hongshui Wang, Fatang Tan, Shitao Li, Materials Letters **60** (2006) 1828–1832

[27] L. Li, H. Yang, H. Zhao et al., "Hydrothermal synthesis and gas sensing properties of single-crystalline ultralong ZnO nanowires," Applied Physics A, vol. **98**, no. 3, pp. 635–641, 2010.

[28]Kim J S, Park W I and Yi G C 2004 ZnO nanorod sensor for detection of biotin-streptavidin interaction unpublished

[29] K. J. Chen, F. Y. Hung, S. J. Chang, and S. J. Young, "Optoelectronic characteristics of UV photodetector based on ZnO nanowire thin films," Journal of Alloys and Compounds, vol. **479**, no. 1-2, pp. 674–677, 2009.

[30] M. H. Huang, S. Mao, H. Feick et al., "Room-temperature ultraviolet nanowire nanolasers," Science, vol. **292**, no. 5523, pp. 1897–1899, 2001. D 245502, 2009.

[31] Harnack O, Pacholski C, Weller H, Yasuda A and Wessels J M 2003 Rectifying behavior of electrically aligned ZnO nanorods *Nano Lett.* **3** 1097

[32] Q. Zhang, C. S. Dandeneau, X. Zhou, and C. Cao, "ZnO nanostructures for dye-sensitized solar cells," Advanced Materials, vol. **21**, no. 41, pp. 4087–4108, 2009.

[33] Q. Zhao, C.-K. Huang, R. Zhu, J. Xu, L. Chen, and D. Yu, "2D planar field emission devices based on individual ZnO nanowires," Solid State Communications, vol. **151**, pp. 1650–1653, 2011.

[34] Arnold M S, Avouris P, Pan Z W and Wang Z L 2003 Field-effect transistors based on single semiconducting oxide nanobelts *J. Phys. Chem.* B **107** 659

[35] C. Ma, Z. Zhou, H. Wei, Z. Yang, Z. Wang, and Y. Zhang, "Rapid large-scale preparation of ZnO nanowires for photocatalytic application," Nanoscale Research Letters, vol. **6**, no. 1, article 536, 2011.

[36] Iowa state university SEM homepage (SEM diagram courtesy)

[37] Purdue university SEM homepage (info courtesy *www.purdue.edu/rem/rs/sem.htm)*

[38] Goldstein, G. I.; Newbury, D. E.; Echlin, P.; Joy, D. C.; Fiori, C.; Lifshin, E. (1981). *Scanning electron microscopy and x-ray microanalysis*. New York: Plenum Press. ISBN 0-306-40768-X.

[39] http://en.wikipedia.org/wiki/Energy-dispersive_X-ray_spectroscopy

[40] Skoog; et al. (2007). *Principles of Instrumental Analysis* (6th ed.). Belmont, CA: Thomson Brooks/Cole. pp. 169–173. ISBN 9780495012016.

[41] Mehta, A. Principle of Ultraviolet-Visible Spectroscopy / http://pharmaxchange.info/press/2011/12/ultraviolet-visible-uv-vis-spectroscopy-principle/

[42] Mehta, A. Derivation of Beer Lambert Law/ http://pharmaxchange.info/press/2012/04/ultraviolet-visible-uv-vis-spectroscopy-%E2%80%93-derivation-of-beer-lambert-law/

[43] http://en.wikipedia.org/wiki/Ultraviolet%E2%80%93visible_spectroscopy

[44] Photoluminescence spectroscopy and its applications module by Ruquan Ye and Andrew R. Barron in Physical Methods in Chemistry and Nanoscience by Andrew R. Barron

[45] http://www.charfac.umn.edu/instruments/d8_advance_overview.html

CHAPTER 3

Study on the effect of recalcination at a higher temperature on the structural and optical properties of ZnO nanoparticles

ABSTRACT

ZnO nanoparticles were successfully synthesized by the simple sol-gel method using precursors zinc acetate dehydrate and potassium hydroxide in ethanol/water solvent. The nanoparticles were calcinated at a temperature of 450°C and recalcinated at 750°C. The structure and morphology of the nanoparticles was analysed by X-Ray Diffraction (XRD) and Scanning Electron Microscope (SEM). For the nanoparticles calcinated at 450°C results reveal that the nanoparticles are agglomerated and possess the hexagonal wurtzite structure. The room temperature photoluminescence (PL) spectrum consists of UV emission and blue emission with twin shoulders at ~409nm and ~430nm due to defect states. The XRD results of the nanoparticles recalcinated at 750°C shows that they retain the hexagonal wurtzite structure. The ZnO nanoparticles are also deagglomerated as confirmed by the SEM results and they become spherical. Recalcination at a higher temperature results in the quenching of visible emission leaving UV emission to dominate at 359nm.

3.1 Introduction

Semiconductor nanomaterials have attracted a lot of interest from various researchers due to their unique size-dependent properties which manifest when a material is reduced from bulk to nanoscale [1-2]. ZnO nanomaterial is one such semiconductor nanomaterial with a wide direct bandgap of 3.37eV and a large exciton energy of 60meV [3-4]. Different morphologies and properties of ZnO nanomaterial can be derived by changing the growth parameters like temperature, pH value, concentration etc [5-7]. The room temperature photoluminescence (PL) of ZnO nanoparticles consists of near band edge (NBE) and visible emission [8-9]. For applications requiring UV emission only visible emission can be eliminated by a thermal post-treatment [10]. Different physical and chemical methods have been used to synthesize ZnO nanoparticles. These methods include RF magnetron sputtering [11], molecular beam

epitaxy [12], electron beam evaporation [13], sol-gel [14], direct precipitation [15], micro-emulsion [16] and solvothermal [17]. The chemical methods are however preferred over physical methods due to low cost, low temperature and simple equipment involved [18-19]. Zinc oxide nanoparticles have a wide range of applications in photocatalysis [20], uv absorbers [21], gas sensing [22], solar cells [23] etc. The performance of different materials and devices incorporating ZnO nanoparticles can however be affected if the nanoparticles are agglomerated [24-25]. Agglomeration has been largely attributed to the method by which the nanoparticles are synthesized and processed [24]. Ball milling, high-shear mixing and ultrasonication are widely applied to deagglomerate nanoparticles [24]. In this study, a post-thermal treatment has been applied to deagglomerate zinc oxide nanoparticles synthesized by the sol-gel method and the effect of recalcination on the structural and optical properties of zinc oxide nanoparticles was investigated by using XRD, SEM, absorption and PL spectroscopy.

3.2 Experimental procedure

All the reagents were of analytical grade and used without further purification. The chemicals were supplied by Rankem Chemicals Ltd. For the synthesis of zinc oxide nanoparticles, 10.097g of zinc acetate dehydrate was dissolved in 100ml ethanol/water solution and heated to 60°C under magnetic stirring. A few drops of ethylene glycol were added and a separate solution made by dissolving 5.16g of potassium hydroxide in double distilled water was then added dropwise and the precursor solution was left to react for 1½ hours with temperature maintained at 60°C. The milky white precipitate formed was then dried in a temperature controlled oven at 120°C for 8 hours to obtain a powder which was calcinated at 450°C for 3 hours in a muffle furnace. Structural and morphological characterization were then performed by X-Ray Diffractometer (Bruker D8 ADVANCE) and Scanning Electron Microscope (HITACHI S-3700N). The powder was used as calcinated and for XRD measurements, CuKα radiation of wavelength λ=1.54Å in the scan range of 5° to 70° for 2Θ was used. Optical characterization was performed by UV/Vis/NIR spectrophotometer (PerkinElmer Lambda 750) and PL spectrofluorometer (HORIBA Jobin Yvon Fluorolog 3 FL3-22). The powder was dissolved in water for the measurement of absorption and PL spectra. The white powder calcinated at 450°C was then recalcinated at a higher temperature

of 750°C for 3 hours. Structural and optical characterization were then repeated and the results were compared at the two different temperatures of 450°C and 750°C.

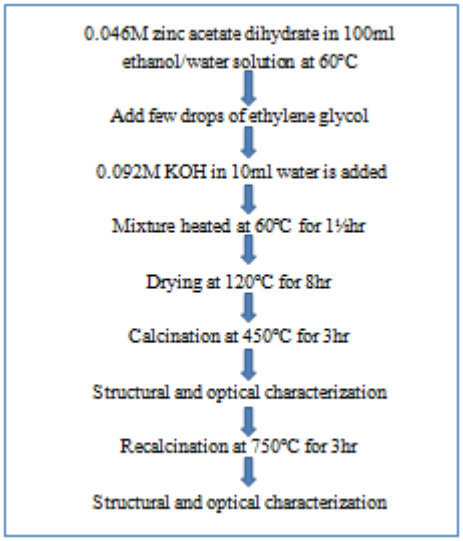

Figure 3.1. Flowchart of the zinc oxide nanoparticles synthesis process

3.3 Results and Discussion

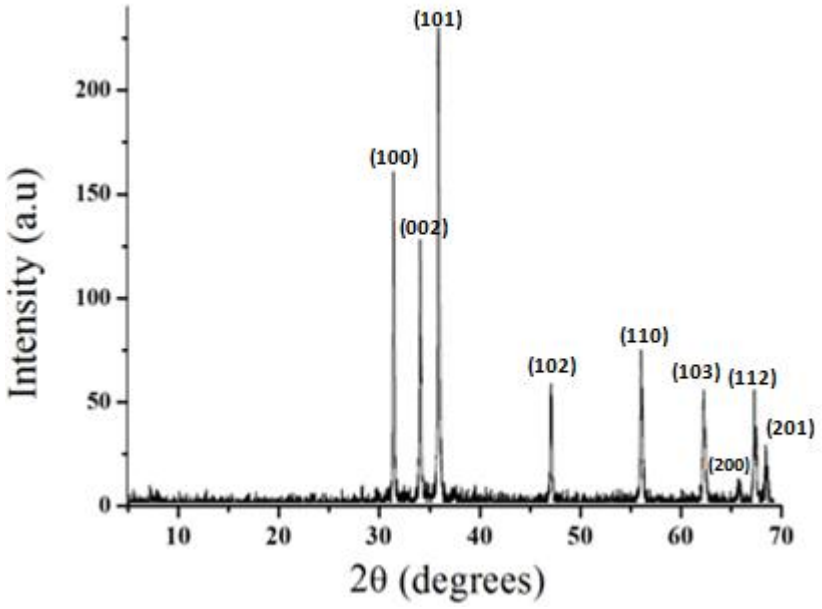

Figure 3.2. XRD spectra of zinc oxide nanoparticles calcinated at 450°C

Figures 3.2 and 3.3 show the XRD pattern of zinc oxide nanoparticles calcinated at 450°C and 750°C respectively. The average crystallite size of the zinc oxide nanoparticles calcinated at 450°C was estimated using the Debye-Scherrer formula [26] and found to be 48nm. The peaks were indexed to the hexagonal wurtzite structure using JCPDS card no. 36-1451. However, there is no impurity peaks detected.

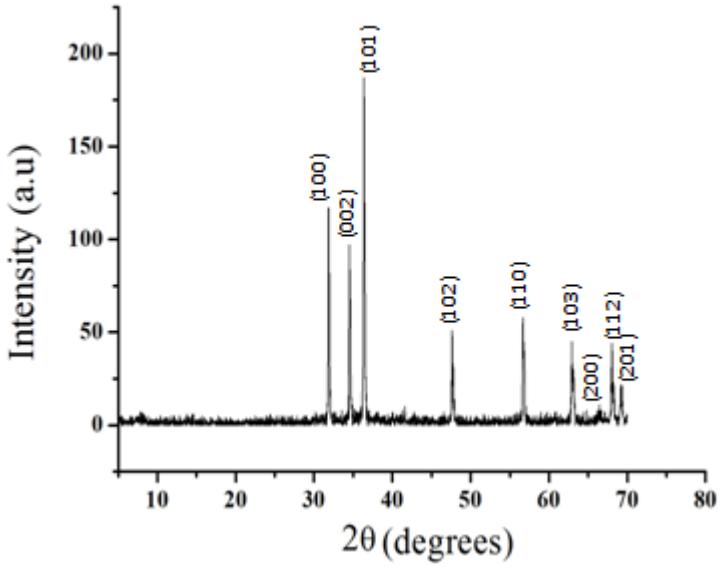

Figure 3.3. XRD spectra of ZnO nanoparticles recalcinated at 750°C

On the other hand, the average crystallite size of the zinc oxide nanoparticles recalcinated at 750°C calculated using the Debye-Scherrer formula was found to be 41nm. The XRD peaks corresponding to the hexagonal wurtzite structure were indexed using JCPDS card no. 36-1451. There were no impurity peaks detected. The sharpness of the peaks confirms the high crystalline quality nature of the zinc oxide nanoparticles.

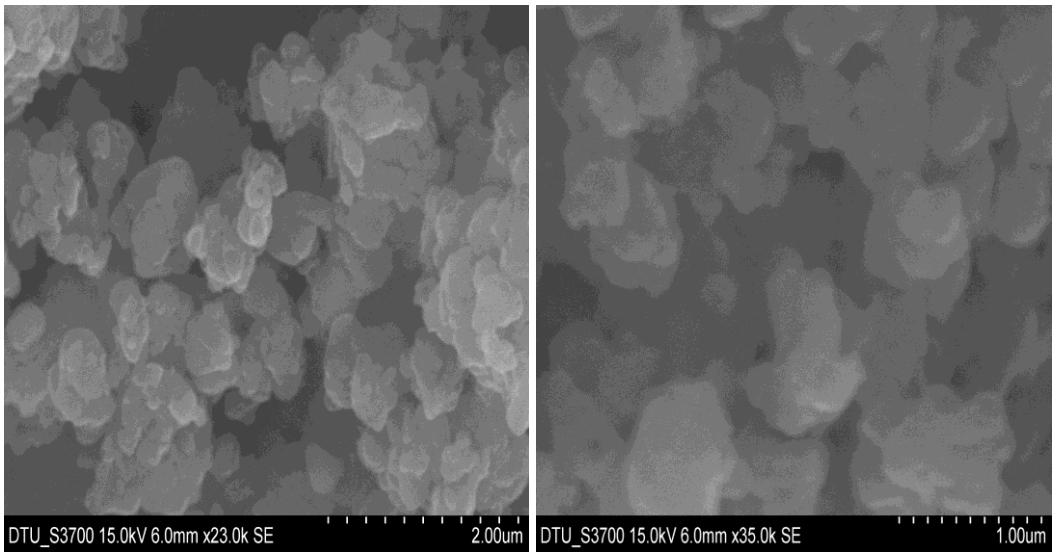

Figure 3.4. SEM images of the zinc oxide nanoparticles calcinated at 450°C

Fig. 3.4 shows SEM images of the zinc oxide nanoparticles calcinated at 450°C. Zinc oxide nanoparticles calcinated at 450°C are highly agglomerated and have an irregular shape with an average particle size around 120nm.

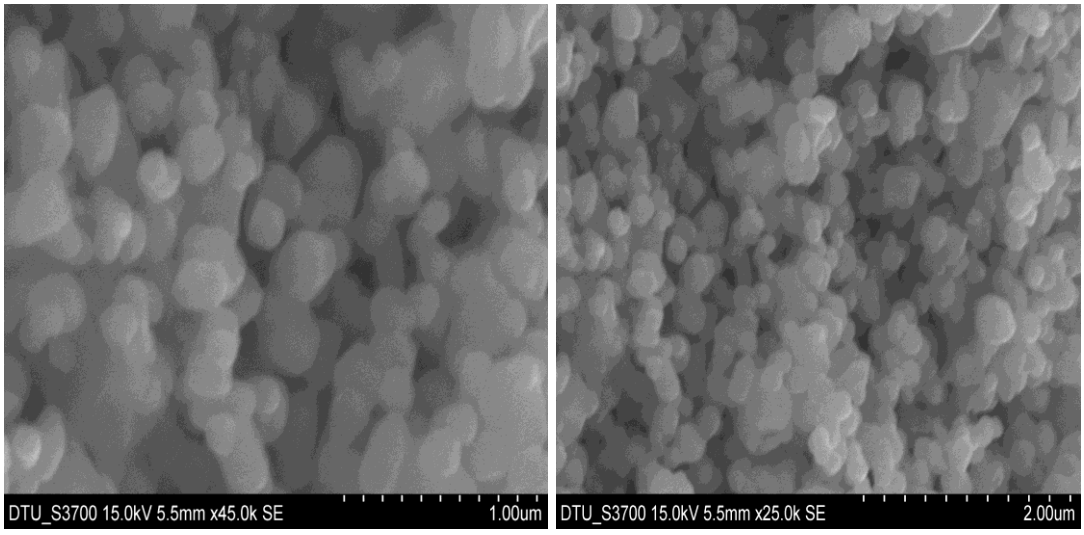

Figure 3.5. SEM images of zinc oxide nanoparticles recalcinated at 750°C

As shown in fig. 3.5, zinc oxide nanoparticles recalcinated at 750°C are free standing with no agglomeration and the particle shape is spherical. The estimated average particle size is around 90nm.

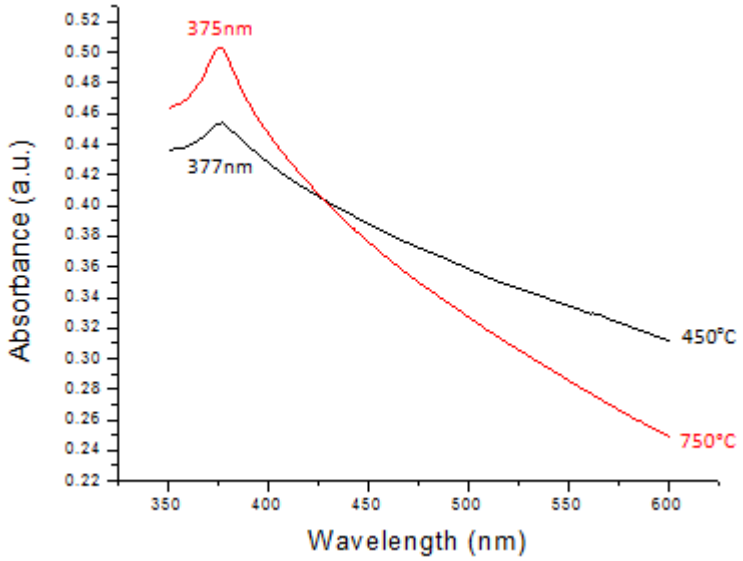

Figure 3.6. Absorption spectra of the zinc oxide nanoparticles

Fig. 3.6 shows the absorption spectra of zinc oxide nanoparticles obtained after calcinated at 450°C and 750°C. As marked in the Figs., the absorption spectra shows peak at 377nm and 375nm at two different calcinated temperatures. The absorption maximum is slightly at higher state than the bulk ZnO, this reflects the quantum confinement effect. The nanoparticles obtained after recalcination at 750°C causes further blue shift in the absorption peak with respect to the 450°C, which confirms the decrease in the particle size.

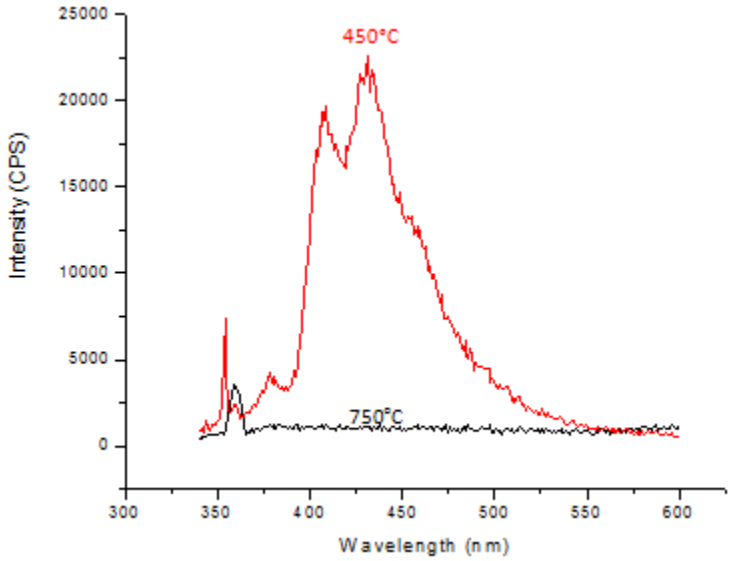

Figure 3.7. Fluorescence spectra of the zinc oxide nanoparticles at λ_{exc} = 320nm

Fig. 3.7 shows the fluorescence spectrum of zinc oxide nanoparticles calcinated at 450°C. The fluorescence spectrum shows peaks at 354nm, 359nm, 378nm, 409nm and 430nm which correspond to UV and blue emission. Recalcination of the nanoparticles at a higher temperature of 750°C eliminates the blue emission resulting in UV emission only at 359nm. A comparison between the properties of ZnO nanoparticles obtained at two different temperatures is given in Table 3.1.

Table 3.1: Summary of comparison of the properties

Property	ZnO NP (450°C)	ZnO NP (750°C)
Structure and phase	Wurtzite (hexagonal phase space group P63mc)	Wurtzite (hexagonal phase space group P63mc)
Agglomeration	Yes	No
Crystallite size (nm)	48	41
Average particle size (nm)	126	90
Particle shape	Undefined	Spherical
Absorption peak (nm)	377 (UV)	375 (UV)
Emission peak (nm)	354,359,378,409,430 (UV & violet)	359 (UV)

3.4 Conclusion

Recalcination of zinc oxide nanoparticles at a higher temperature of 750°C altered the structural and optical properties of the nanoparticles calcinated at 450°C. The nanoparticles are deagglomerated and become spherical at 750°C. The structure and phase however is unchanged. The absorption peak is blue shifted when the nanoparticles are recalcinated at higher temperature, which is due to a reduction in the particle size. At 750°C, ZnO nanomaterials became defect free. The defect-related states are eliminated, resulting in UV emission only at 359nm. Thus post-thermal treatment at a higher temperature can also be an effective way to deagglomerate nanoparticles and to reduce/eliminate defects-related states allowing the material potential use in UV-based optoelectronic applications.

References

[1] Nel A, Xia T, Madler L, Li N. Toxic potential of materials at the nanolevel. Science. 2006:**311**:622-7

[2] Grégory Guisbiers, Sergio Mejía-Rosales, and Francis Leonard Deepak, "Nanomaterial Properties: Size and Shape Dependencies," Journal of Nanomaterials, vol. **2012**, Article ID 180976, 2 pages, 2012.

[3] Zhong Lin Wang, Zinc oxide nanostructures: growth, properties applications, 2004 J. Phys.: Condens. Matter **16** R829-R858

[4] Manikandan E, Moodley MK, Sinha Ray S, Panigrahi BK, Krishnan R, Padhy N, Nair KG, Tyagi AK. Zinc oxide epitaxial thin film deposited over carbon on various substrate by pulsed laser deposition technique. J Nanosci Nanotechnol. 2010 Sep;**10**(9):5602-11.

[5] Jinzhou Yin, Feng Gao, Chengzhen Wei, and Qingyi Lu. (2014). Water Amount Dependence on Morphologies and Properties of ZnO nanostructures in Double-solvent System. *Scientific Reports*; Volume: **4**,; Article number: 3736.

[6] Linping Xu, Yan-Ling Hu, Candice Pelligra, Chun-Hu Chen, Lei Jin, Hui Huang, Shanthakumar Sithambaram, et al. (2009). ZnO with Different Morphologies Synthesized by Solvothermal Methods for Enhanced Photocatalytic Activity. Chemistry of Materials. 2009 Vol: **21**(13):2875-2885.

[7] Xinyu Zhang, Jiaqian Qin, Yanan Xue, Pengfei Yu, Bing Zhang, Limin Wang, and Riping Liu. (2014). Effect of aspect ratio and surface defects on the photocatalytic activity of ZnO nanorods. Scientific Reports; Volume: **4**,; Article number: 4596.

[8] Noh Soo Han, Hyeong Seop Shim, Joo Hee Seo, Sun Young Kim, Seung Min Park and Jae Kyu Song.Defect states of ZnO nanoparticles: Discrimination by time-resolved photoluminescence spectroscopy. J. Appl. Phys. **107**, 084306 (2010)

[9] Magnus Willander , Omer Nur, Jamil Rana Sadaf, Muhammad Israr Qadir, Saima Zaman, Ahmed Zainelabdin, Nargis Bano and Ijaz Hussain. Luminescence from Zinc Oxide Nanostructures and Polymers and their Hybrid Devices. Materials 2010, **3**, 2643-2667

[10] Spanhel L 2006 J.Sol-Gel Sci: Technol. **39** 7

[11] Q.P. Wang, D.H. Zhang, Z.Y. Xue, X.T. Hao. Violet luminescence emitted from ZnO films deposited on Si substrate by RF magnetron sputtering. Appl. Surf. Sci., **201** (2002), pp. 123–128

[12] M. S. Kim, G. Nam, J. S. Son, and J. Y. Leem, "Photoluminescence studies of ZnO thin films on porous silicon grown by plasma-assisted molecular beam epitaxy," Current Applied Physics, vol. **12**, supplement 4, pp. S94–S98, 2012.

[13] M. G. Varnamkhasti, H. R. Fallah, and M. Zadsar, "Effect of heat treatment on characteristics of nanocrystalline ZnO films by electron beam evaporation," Vacuum, vol. **86**, no. 7, pp. 871–875, 2012.

[14] Y. L. Zhang; Y. Yang; J. H. Zhao; R. Q. Tan; P. Cui; W. J. Song. Preparation of ZnO nanoparticles by a surfactant-assisted complex sol–gel method using zinc nitrate. Journal of Sol-Gel Science and Technology 2009 Vol: **51**(2):198-203.

[15] A. H. Moharram, S. A. Mansour, M. A. Hussein and M. Rashad. Direct Precipitation and Characterization of ZnO Nanoparticles. Journal of Nanomaterials Volume **2014**, Article ID 716210, 5 pages, 2014

[16] S. López-Cuenca, M. Rabelero, H. Saade, R. G. López, E. Mendizábal, and J. E. Puig, "High-yield synthesis of zinc oxide nanoparticles from bicontinuous microemulsions," Journal of Nanomaterials, vol. **2011**, Article ID 431382, 6 pages, 2011

[17] Jiabiao Lian, Yao Liang, Fung-luen Kwong, Zhimin Ding, Dickon H.L. Ng. Template-free solvothermal synthesis of ZnO nanoparticles with controllable size and their size-dependent optical properties. Mater. Lett. **66**, 318-320 (2012)

[18] Gnanasangeetha D.and SaralaThambavani D. One Pot Synthesis of Zinc Oxide Nanoparticles via Chemical and Green Method. Res.J.Material Sci. Vol.**1**(7), 1-8 (2013)

[19] Zafar Hussain Ibupoto, Kimleang Khun, Martin Eriksson, Mohammad AlSalhi, Muhammad Atif , Anees Ansari and Magnus Willander**.** Hydrothermal Growth of Vertically Aligned ZnO Nanorods using a Biocomposite Seed layer of ZnO Nanoparticles *Materials* 2013***, 6***, 3584-3597

[20] Giraldi TR, Santos GV, Mendonça VR, Ribeiro C, Weber IT. J Nanosci Nanotechnol. 2011 Apr;**11**(4):3635-40. Annealing effects on the photocatalytic activity of ZnO nanoparticles.

[21] Lansdown, A. B. G.; Taylor, A. Zinc and titanium oxides: promising UV-absorbers but what influence do they have on the intact skin? Int. J. Cosmet. Sci. **19,** 167-172 (1997) .

[22] Rao, G. S. T. & Rao, D. T. Gas sensitivity of ZnO based thick film sensor to NH_3 at room temperature. Sens. Actuat. B **55**, 166–169 (1999).

[23] Ka Kan Wong et al. Effect of ZnO Nanoparticle Properties on Dye-Sensitized Solar Cell Performance. ACS Appl. Mater. Interfaces, 2012, **4** (3), pp 1254–1261

[24] Bertrand Faure et al. Dispersion and surface functionalization of oxide nanoparticles for transparent photocatalytic and UV-protecting coatings and sunscreens. Sci. Technol. Adv. Mater. **14** (2013) 023001

[25] Lennart Bergström, Colloidal processing of ceramics, 2001, Handbook of Applied Surface and Colloid Chemistry, Chapter 9, 201-218

[26] Satyanarayana Talam, Srinivasa Rao Karumuri, and Nagarjuna Gunnam, "Synthesis, Characterization, and Spectroscopic Properties of ZnO Nanoparticles," ISRN Nanotechnology, vol. **2012**, Article ID 372505, 6 pages, 2012.

CHAPTER 4

Temperature dependence growth of ZnO nanocapsules using directional agent EDA

ABSTRACT

Short ZnO nanorods with different aspect ratios were successfully synthesized by the simple sol-gel method at different temperatures using the shape-directing agent EDA. The morphology of the nanorods was analysed by Scanning Electron Microscope (SEM). Results reveal that the nanorods synthesized at 450°C have a diameter of ~40nm and a length of ~300nm. Increasing the calcination temperature to 600°C reduces their aspect ratio hence confirming the temperature-dependence growth of the synthesized ZnO nanorods. The decrease in the aspect ratio was also confirmed by absorption spectrum, which shows a red shift when the ZnO nanorods are calcinated at 600°C. The room temperature photoluminescence (PL) spectrum consists of UV and blue emission for both samples with no considerable difference in the emission peak positions.

4.1 Introduction

1D nanostructures have unique properties due to the quantum confinement effect and the large surface to volume ratio they exhibit [1-2]. ZnO is a group II-VI semiconductor with a wide bandgap of 3.37eV and a large exciton binding energy of 60meV at room temperature [3-4] that exhibits near band edge (NBE) emission and visible emission [5-6]. The NBE emission is due to free excitonic recombinations whereas visible emission is due to defect states [7]. The defects present in ZnO nanostructures determine their optoelectronic properties, which has an impact in material and device applications [8]. ZnO nanorods have a wide range of applications which include UV lasers [9], solar cells [10], field emission devices [11], field effect transistors (FETs) [12], LEDs [13]. Several methods such as CVD [14], laser ablation [15], hydrothermal [16], spray pyrolysis [17], sol-gel [18] and sputtering [19] have been used to synthesize ZnO nanorods. Wet chemical methods are however preferred over the physical methods due to the cost

effectiveness and simple equipment involved [20]. Additives such as EDA can also be introduced at some instances to promote one-dimensional growth [16]. The effect of different parameters such as concentration, pH value, temp etc on the morphology and properties of ZnO nanorods has been studied by different researchers [21-24]. Zhang et al. [25] have studied the effect of aspect ratio and surface defects on the photocatalytic activity of ZnO nanorods synthesized by the mechanical-assisted thermal decomposition method in which they discovered that the calcination temperature has an effect on the aspect ratio of the synthesized nanorods. In this work, the effect of the calcination temperature on the morphology and optical properties of the ZnO nanorods grown by a simple wet chemical method (sol-gel) has been investigated.

4.2 Experimental procedure

All the reagents were of analytical grade and used without further purification. The chemicals were supplied by Rankem Chemicals Ltd. For the synthesis of zinc oxide nanocapsules, 10.975g of zinc acetate dehydrate was dissolved in 100ml double distilled water and 10ml of EDA was added under magnetic stirring at 75°C. A separate solution was prepared by dissolving 5.611g of potassium hydroxide in 10ml of double distilled water and added dropwise and the mixture was left to react for 2 hours. The milky white precipitate formed was then dried in a temperature controlled oven at 120°C for 8 hours to obtain a white powder which was divided into two portions and calcinated at two different temperatures of 450°C and 600°C for 3 hours in a muffle furnace. Morphological characterization were then perfomed by Scanning Electron Microscope (HITACHI S-3700N). The powder was used as calcinated. Optical characterization was performed by UV/Vis/NIR spectrophotometer (PerkinElmer Lambda 750) and PL spectrofluorometer (HORIBA Jobin Yvon Fluorolog 3 FL3-22). The powder was dissolved in water solvent for both UV/Vis and PL spectroscopy. The results were then compared for the two samples calcinated at different temperatures of 450°C and 600°C.

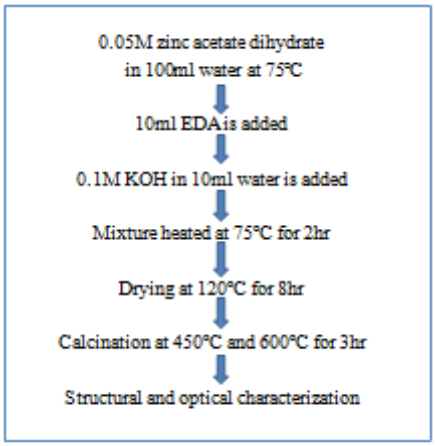

Figure 4.1. Flowchart of the zinc oxide nanocapsules synthesis process

4.3 Results and Discussion

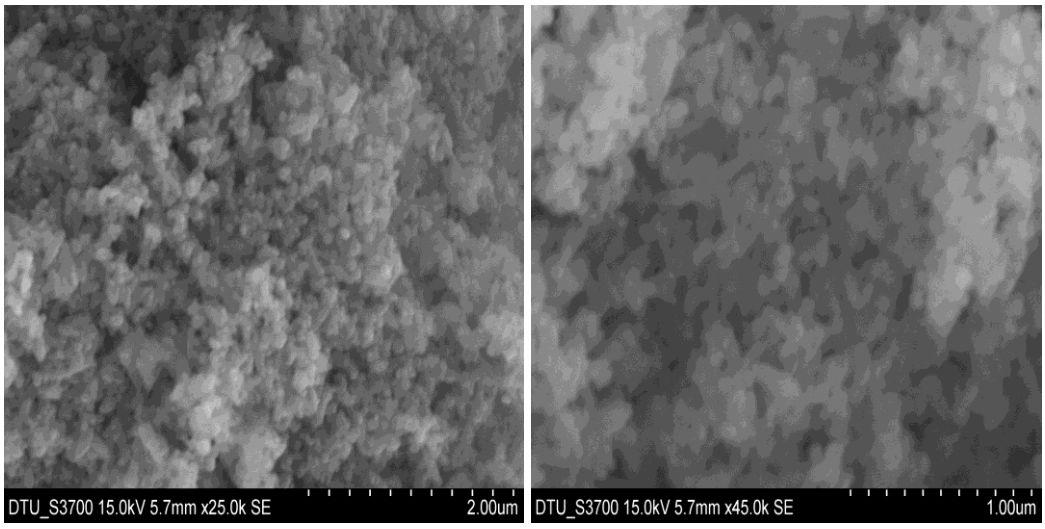

Figure 4.2. SEM images of the zinc oxide nanocapsules synthesized at 450°C

The SEM images of zinc oxide nanocapsules synthesized at 450°C and 600°C are shown in Figures 4.2 and 4.3. The diameter and length of the synthesized ZnO nanocapsules (450°C) are about 40nm and 300nm respectively. In addition, there are also spherical nanoparticles with diameters around 50nm.

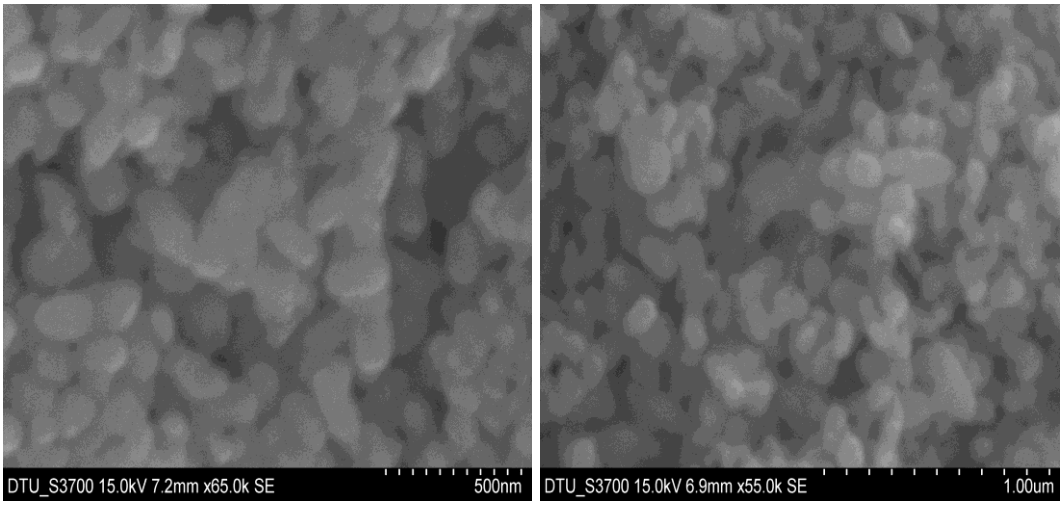

Figure 4.3. SEM images of zinc oxide nanocapsules synthesized at 600°C

However, the diameter and length of the zinc oxide nanocapsules critically depend on the calcination temperature. ZnO nanocapsules synthesized at 600°C have diameters around 100nm and lengths of up to 250nm.

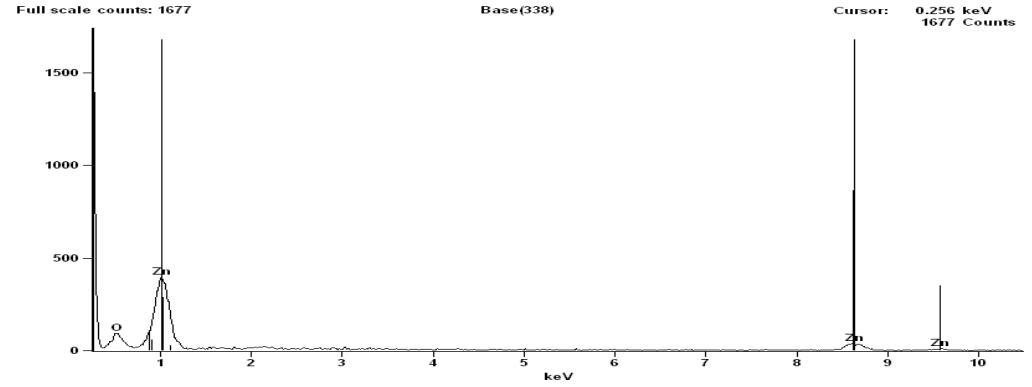

Element Line	Net Counts	Int. Cps/nA	Weight %	Weight% Error	Atom %	Atom % Error	Formula
O K	6309	---	20.85	+/- 0.43	51.84	+/- 1.08	O
Zn K	2847	---	79.15	+/- 3.84	48.16	+/- 2.33	Zn
Zn L	20818	---	---	---	---	---	
Total			100.00		100.00		

Figure 4.4. EDX spectra of the zinc oxide nanocapsules calcinated at 450°C

Figure 4.4 shows the EDX spectra of the zinc oxide nanocapsules calcinated at 450°C. The elemental peaks corresponding to zinc and oxygen were detected. The elemental composition corresponding to the peak intensities is larger for zinc element as compared to that of oxygen. No impurity peaks were detected.

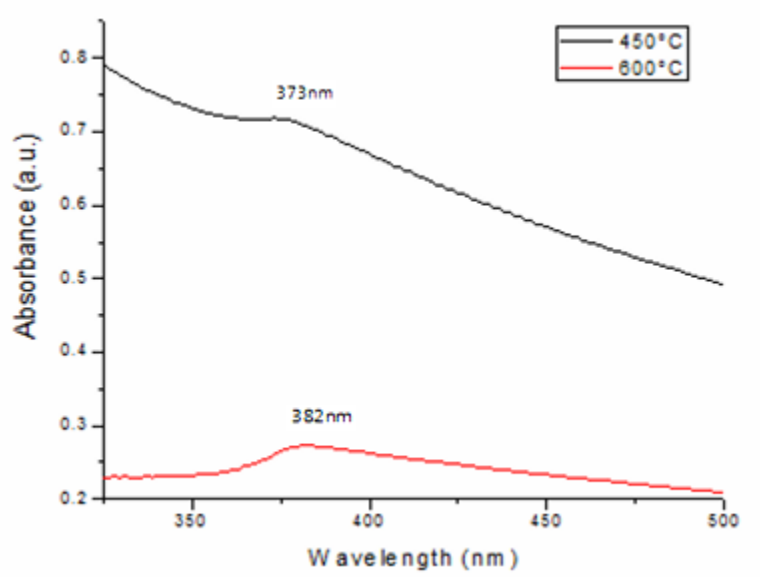

Figure 4.5. Absorption spectra of zinc oxide nanocapsules

Zinc oxide nanocapsules synthesized at 450°C have an absorption peak at 373nm (Fig. 4.5) which is at much lower wavelength than that of bulk zinc oxide (380nm) due to the quantum confinement effect. Increasing the calcination temperature to 600°C shifts the absorption peak to 382nm, due to an increase in the particle diameter.

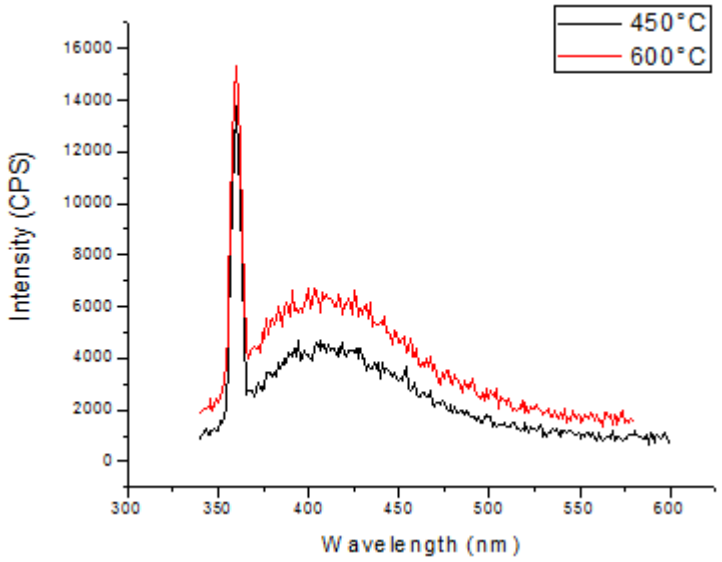

Figure 4.6. PL spectra of the zinc oxide nanocapsules at λ_{exc} = 320nm

For both samples, the photoluminescence (PL) spectra obtained with 320nm excitation shows two emission peaks at 360nm and 406nm corresponding to UV and blue emission, respectively. The UV emission peak is larger than that for the blue emission confirming the fewer defects in the two materials. There is however no significant change in the UV and blue emission peak positions.

4.4 Conclusion

Zinc oxide nanorods with short lengths were successfully grown using EDA capping agent, which promotes one-dimensional growth. The shorter nanorods were a result of a short growth time of two hours. Increasing the calcination temperature from 450°C to 600°C reduces the aspect ratio of the nanorods, with no significant change in the UV and blue emission peak positions. The material has potential use in UV and visible emission devices.

References

[1] Y. Xia, P. Yang, Y. Sun et al., "One-dimensional nanostructures: synthesis, characterization, and applications," Advanced Materials, vol. **15**, no. 5, pp. 353–389, 2003.

[2] Grégory Guisbiers, Sergio Mejía-Rosales, and Francis Leonard Deepak. "Nanomaterial Properties: Size and Shape Dependencies", Journal of Nanomaterials, Volume **2012** (2012), Article ID 180976, 2 pages

[3] F. Lu, W. Cai, and Y. Zhang, "ZnO hierarchical micro/nanoarchitectures: solvothermal synthesis and structurally enhanced photocatalytic performance," Advanced Functional Materials, vol. **18**, no. 7, pp. 1047–1056, 2008.

[4] Q. Humayun, M. Kashif, and U. Hashim, "Structural, Optical, Electrical, and Photoresponse Properties of Postannealed Sn-Doped ZnO Nanorods," Journal of Nanomaterials, vol. **2013**, Article ID 792930, 8 pages, 2013.

[5] Gyu-Chul Yi, Chunrui Wang and Won Il Park. ZnO nanorods: synthesis,characterization and applications Semicond. Sci.Technol. **20** (2005) S22–S34

[6] P. Kathirvel, J. Chandrasekaran, D. Manoharan, S. Kumar. Formation and characterization of flame synthesized hexagonal zinc oxide nanorods for gas sensor applications. Ceramics International Volume **39**, Issue 5, July 2013, Pages 5321–5325

[7] A. Gupta, M. Omari and N. Kouklin. Spectral investigation of carrier recombination processes in ZnO nanorods at high temperatures. J. Appl. Phys. **103**, 124312

[8] J. G. Reynolds, C. L. Reynolds Jr., A. Mohanta, J. F. Muth, J. E. Rowe, H. O. Everitt and D. E. Aspnes. Shallow acceptor complexes in p-type ZnO . Appl. Phys. Lett. **102**, 152114

[9] Huang, M. H. *et al.* Room-temperature ultraviolet nanowire nanolasers. Science **292**, 1897–1899 (2001).

[10] P. Sudhagar, R. S. Kumar, J. H. Jung et al., "Facile synthesis of highly branched jacks-like ZnO nanorods and their applications in dye-sensitized solar cells," Materials Research Bulletin, vol. **46**, no. 9, pp. 1473–1479, 2011

[11] Lee C J, Lee T J, Lyu S C, Zhang Y, Ruh H and Lee H J 2002 Field emission from well-aligned zinc oxide nanowires grown at low temperature *Appl. Phys. Lett.* **81** 3648

[12] Arnold, M. S., Avouris, P., Pan, Z. W. & Wang, Z. L. Field-effect transistors based on single semiconducting oxide nanobelts. J. Phys. Chem. B **107**, 659–663 (2003).

[13] Shrawan Jha *et al* Violet-blue LEDs based on p-GaN/n-ZnO nanorods and their stability. 2011 *Nanotechnology* **22** 245202

[14] Xiang Liu, Xiaohua Wu, Hui Cao and R. P. H. Chang. Growth mechanism and properties of ZnO nanorods synthesized by plasma-enhanced chemical vapor deposition. J. Appl. Phys. **95**, 3141

[15] Tatsuo Okada, Kou Kawashima, Yoshiki Nakata and Xu Ning. 2005. Synthesis of ZnO Nanorods by Laser Ablation of ZnO and Zn Targets in He and O_2 Background Gas. *Jpn. J. Appl. Phys.* **44** 688

[16] Bin Liu and Hua Chun Zeng. Hydrothermal Synthesis of ZnO Nanorods in the Diameter Regime of 50 nm. *J. Am. Chem. Soc.*, 2003, **125** (15), pp 4430–4431

[17] Kärber E, Raadik T, Dedova T, Krustok J, Mere A, Mikli V, Krunks M. Photoluminescence of spray pyrolysis deposited ZnO nanorods. Nanoscale Res Lett. 2011 Apr 21;**6**(1):359.

[18] Seung Eon Ahn et al. Photoresponse of sol-gel-synthesized ZnO nanorods. Appl. Phys. Lett. **84**, 5022 (2004)

[19] P. Sundara Venkatesh, C.L. Dong, C.L. Chen, W.F. Pong, K. Asokan, K. Jeganathan. Local electronic structure of ZnO nanorods grown by radio frequency magnetron sputtering. 2014. Mater. Lett. **116**, 206–208

[20] Yangyang Zhang, Manoj K. Ram, Elias K. Stefanakos, and D. Yogi Goswami, "Synthesis, Characterization, and Applications of ZnO Nanowires," Journal of Nanomaterials, vol. **2012**, Article ID 624520, 22 pages, 2012.

[21] Kim AR, Lee JY, Jang BR, Lee JY, Kim HS, Jang NW. Effect of Zn2+ source concentration on hydrothermally grown ZnO nanorods. J Nanosci Nanotechnol. 2011 Jul;**11**(7):6395-9.

[22] Cho MY, Kim MS, Yim KG, Lee DY, Kim JS, Kim JS, Leem JY. Effects of precursor concentrations and thermal annealing on ZnO nanorods grown by hydrothermal method. J Nanosci Nanotechnol. 2011 Aug;**11**(8):7479-82.

[23] Effects of annealing temperature on photoluminescence of ZnO nanorods hydrothermally grown on a ZnO:Al seed layer. 2013. Optical Materials, **35**(12), 2649-2653.

[24] Zhang, L., Ruan, Y., Liu, Y. and Zhai, Y. (2013), Effect of growth temperature on the structure and optical properties of ZnO nanorod arrays grown on ITO substrate. Cryst. Res. Technol., **48**: 996–1002.

[25] Zhang, X.Y. et al. Effect of aspect ratio and surface defects on the photocatalytic activity of ZnO nanorods. Sci. Rep. **4**, 4596.

CHAPTER 5

Growth of self-assembled ZnO nanoflowers by the sol-gel process

ABSTRACT

Self-assembled ZnO nanoflowers were successfully synthesized by the simple sol-gel method using distilled water as medium and EDA as capping agent. The structure and morphology of the ZnO nanoflowers were analysed by using X-Ray Diffraction (XRD) and Scanning Electron Microscope (SEM). The XRD pattern revealed the hexagonal wurtzite structure and the SEM images show the presence of bullet-shaped nanorods having tip diameters up to 80nm and lengths up to 1μm. The absorption at ~264nm exhibits quantum confinement effect. The room temperature photoluminescence (PL) spectrum consists of UV emission and blue emission at 360nm and 430nm, respectively. The UV emission is attributed to excitonic radiative recombination whereas the blue emission is caused by defect states.

5.1 Introduction

ZnO as a semiconductor material with a direct wide bandgap of 3.37eV and high exciton binding energy of 60meV [1-4] has attracted a lot of attention from researchers due to its unique properties at the nanoscale [5] and wide range of applications in LEDs [6], FETs [7], photocatalysis [8], UV lasers [9] and solar cells [10]. The morphologies and properties of ZnO nanostructures can easily be tailored by changing the growth parameters like temperature, pH, concentration, time etc. [11-15]. 1D ZnO nanostructures which include nanowires [16], nanorods [17-18], nanotubes [19-20] have been synthesized by different methods such as hydrothermal, sol-gel, thermal evaporation and sputtering. Various research groups have synthesized flower-like ZnO nanostructures composed of self-assembled nanorods using different methods and conditions [21-29]. In this work, the synthesis of self assembled ZnO nanoflowers by using a simple wet chemical method assisted by a capping agent, EDA, is reported. This method exhibits several advantages over the physical methods like low cost and also requires simple equipment [30]. The structure, morphology and optical properties of the synthesized flower-like ZnO nanostrures were characterized by using XRD, SEM, EDX, optical absorption and PL spectroscopy.

5.2 Experimental procedure

All the reagents used were of analytical grade and without further purification. The chemicals were obtained from Rankem Chemicals Ltd. For the synthesis of self assembled zinc oxide nanoflowers, 10.975g of zinc acetate dehydrate was dissolved in 100ml of double distilled water and 10ml of EDA was added under magnetic stirring at 75°C. A separate solution prepared by dissolving 5.611g of potassium hydroxide in 10ml of double distilled water was then added dropwise and the mixture was left to react for 6 hours with temperature maintained at 75°C. The milky white precipitate formed was dried in an oven at 120°C for 5 hours and further calcinated at 450°C for 3 hours in a muffle furnace. Structural and morphological characterization were then perfomed by X-Ray Diffractometer (Siemens D-500) and Scanning Electron Microscope (HITACHI S-3700N). The powder was used as calcinated and for XRD measurements, CuKα radiation of wavelength λ=1.54Å in the scan range of 5° to 70° for 2Θ was used. Optical characterization was performed by UV/Vis/NIR spectrophotometer (PerkinElmer Lambda 750) and PL spectrofluorometer (HORIBA Jobin Yvon Fluorolog 3, FL3-22). The powder was dissolved in water solvent and the excitation wavelength was 320nm for both UV/Vis and PL spectroscopy. The results were then analysed.

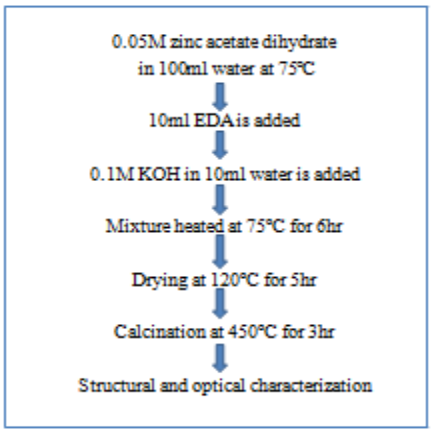

Figure 5.1. Flowchart of the zinc oxide nanoflowers synthesis process

5.3 Results and Discussion

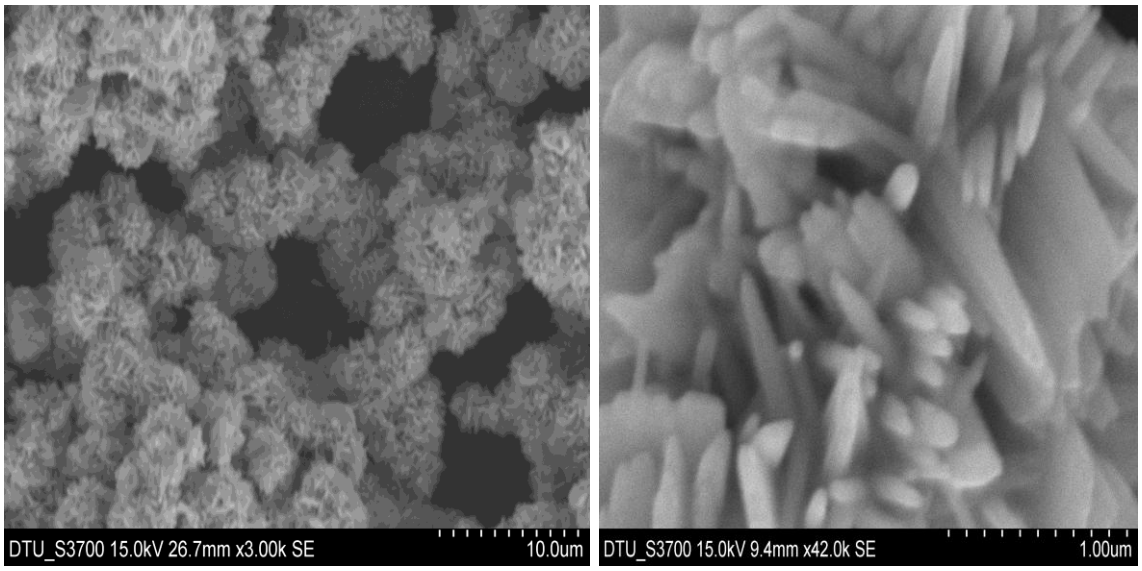

Figure 5.2. SEM images of the zinc oxide nanoflowers

Fig. 5.2 shows the SEM image of the synthesized zinc oxide nanoflowers obtained after calcination at 450°C. The zinc oxide nanoflowers clusters are almost spherical and these clusters are composed of bullet-shaped nanorods stacked together and the nanorods growth is also from a common central point. The nanorods have tip diameters up to 80nm and lengths up to 1µm.

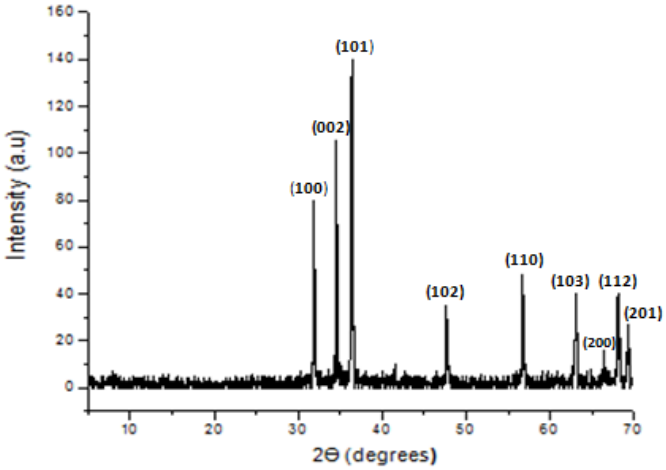

Figure 5.3. XRD of the zinc oxide nanoflowers

Fig. 5.3 shows the XRD pattern. The peaks were indexed to the hexagonal wurtzite structure following JCPDS card no. 80-0075. No impurity peaks were detected.

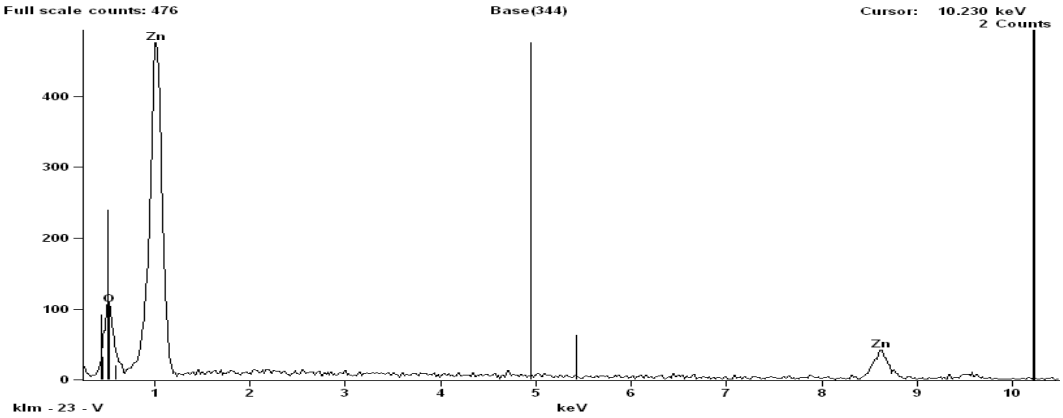

Element Line	Net Counts	Int. Cps/nA	Weight %	Weight% Error	Atom %	Atom % Error	Formula
O K	1634	---	20.79	+/- 0.67	51.75	+/- 1.68	O
Zn K	741	---	79.21	+/- 7.06	48.25	+/- 4.30	Zn
Zn L	6179	---	---	---	---	---	
Total			100.00		100.00		

Figure 5.4. EDX spectra of the zinc oxide nanoflowers

The strong elemental peaks detected correspond to zinc and oxygen in the EDS of ZnO nanoflowers, as shown in Fig. 5.4. No impurity peaks were detected and the elemental composition is higher for zinc compared to oxygen element.

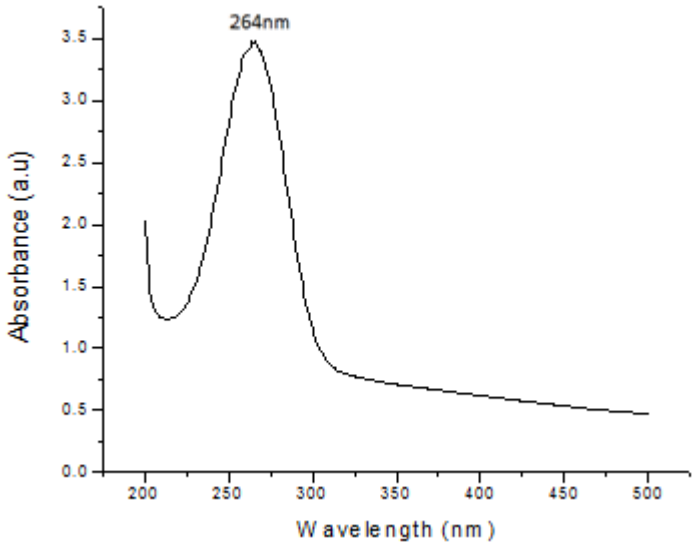

Figure 5.5. Absorption spectra of the synthesized zinc oxide nanoflowers

The absorption spectrum shows a peak at 264nm for the zinc oxide nanoflowers. The shorter wavelength absorption is obtained due to the quantum confinement effect.

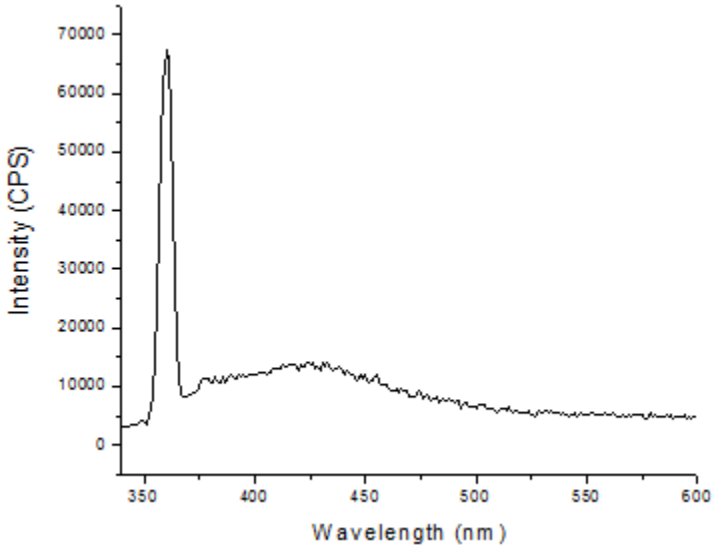

Figure 5.6. PL spectra of the zinc oxide nanoflowers at λ_{exc} = 320nm

Fig. 5.6 shows the photoluminescence spectrum of ZnO nanoflowers with 320nm excitation. The spectra shows two emission bands at 360nm and 430nm corresponding to

UV emission and blue emission respectively. The blue emission peak is smaller than that of the UV emission confirming the fewer defects in the material synthesized at 450°C.

5.4. Conclusion

Self-assembled zinc oxide nanoflowers were successfully grown by the sol-gel process at a growth time of 6hrs using water solvent. The nanoflowers show an absorption peak at 260nm, which is far below to the 380nm obtained for the bulk zinc oxide. This large blue shifted absorption is obtained due to the quantum confinement effect and the dominant UV emission over visible emission gives the material potential use in UV-based optoelectronic devices.

References

[1] Anderson Janotti and Chris G Van de Walle. Fundamentals of zinc oxide as a semiconductor. 2009. *Rep. Prog. Phys.* **72** 126501

[2] Klingshirn, C. (2007), ZnO: Material, Physics and Applications. ChemPhysChem, **8**: 782–803.

[3] S. Tüzemen, E. Gür, Yıldırım, T., G. Xiong, and R. T. Williams, An investigation of control mechanisms of the excitonic behavior in reactively sputtered ZnO on (0001) Al_2O_3. J. Appl. Phys. **100**, 103513 (2006).

[4] Lyu, S. C. , Zhang, Y., Ruh, H., Lee, H. J. , Shim, H. W. , Suh, E. K. , and Lee, C., Low temperature growth and photoluminescence of well-aligned zinc oxide nanowires. J. Chem. Phys. Lett. **363**, 134–138 (2002).

[5] Megan M. Brewster, Xiang Zhou, Ming-Yen Lu and Silvija Gradečak. The interplay of structural and optical properties in individual ZnOnanostructures. ***Nanoscale***, 2012,**4**, 1455-1462

[6] Miin-Jang Chen, Jer-Ren Yang and Makoto Shiojiri. ZnO-based ultra-violet light emitting diodes and nanostructures fabricated by atomic layer deposition 2012 *Semicond. Sci. Technol.* **27** 074005

[7] Atanasova, P., Rothenstein, D., Schneider, J. J., Hoffmann, R. C., Dilfer, S., Eiben, S., Wege, C., Jeske, H. and Bill, J. (2011), Virus-Templated Synthesis of ZnO Nanostructures and Formation of Field-Effect Transistors. Adv. Mater., **23**: 4918–4922.

[8] Linhua Xu, Gaige Zheng, Junfeng Wang, Min Lai, Juhong Miao, Fenglin Xian, Fang Gu, Tingting Sun. Leaf-like ZnO nanostructure and its excellent photocatalytic activity. Mater. Lett. **122**, 1-4

[9] Huang M H, Mao S, Feick H, Yan H Q, Wu Y Y, Kind H, Weber E, Russo R and Yang P D 2001 Room-temperature ultraviolet nanowire nanolasers. *Science.* **292** 1897

[10] Greene, L. E.; Law, M; Tan, DH; Montano, M; Goldberger, J; Somorjai, G; Yang, P (2005). "General Route to Vertical ZnO Nanowire Arrays Using Textured ZnO Seeds". *Nano Letters* **5** (7): 1231–1236.

[11] Zhang, X.Y. et al. Effect of aspect ratio and surface defects on the photocatalytic activity of ZnO nanorods. Sci. Rep. **4**, 4596.

[12] B. Cheng and E. T. Samulski, "Hydrothermal synthesis of one-dimensional ZnO nanostructures with different aspect ratios," Chemical Communications, vol. **10**, no. 8, pp. 986–987, 2004.

[13] S. Baruah and J. Dutta, "pH-dependent growth of zinc oxide nanorods," Journal of Crystal growth, **311** (8), 2549–2554 (2009)

[14] Xufeng Wu, Hua Bai, Chun Li, Gewu Lu and Gaoquan Shi**.** Controlled one-step fabrication of highly oriented ZnO nanoneedle/nanorods arrays at near room temperature. *Chem. Commun.*, 2006, 1655-1657

[15] Rai P, Jo JN, Wu XF, Yoon JM, Yu YT. Synthesis of well dispersed, regular shape ZnO nanorods: effect of pH, time and temperature. J Nanosci Nanotechnol. 2011; **11**(1): 647-651.

[16] J B Baxter, A M Walker, K van Ommering and E S Aydil. Synthesis and characterization of ZnO nanowires and their integration into dye-sensitized solar cells. 2006 *Nanotechnology* **17** S304

[17] Hongxia Zhang, Jing Feng, Jun Wang, Minlin Zhang. Preparation of ZnO nanorods through wet chemical method. Mater. Lett. **61**, 5202-5205

[18] Seung Eon Ahn et al. Photoresponse of sol-gel-synthesized ZnO nanorods. Appl. Phys. Lett. **84**, 5022 (2004)

[19] Xing.J.Y et al. Optical properties of the ZnO nanotubes synthesized via vapor phase growth. Appl. Phys. Lett. **83**, 1689 (2003)

[20] Tuğba İpeksaç, Figen Kaya, Cengiz Kaya. Hydrothermal synthesis of Zinc oxide (ZnO) nanotubes and its electrophoretic deposition on nickel filter. Mater. Lett. **100**, 11-14 (2013)

[21] Jiu-Ju Feng, Zhen-Zhen Wang, Yong-Fang Li, Jian-Rong Chen and Ai-Jun Wang. Control growth of single crystalline ZnO nanorod arrays and nanoflowers with enhanced photocatalytic activity. ***J Nanopart Res***, 2013, **15** (4).

[22] Zheng, J. H.; Jiang, Q.; Lian, J. S. Synthesis and optical properties of flower-like ZnO nanorods by thermal evaporation method. *Appl. Surf. Sci.* **257,** 5083-5087 (2011) .

[23] Al-Hajry A. Low-temperature growth and dye-sensitized solar cells applications of flower-shaped ZnO hexagonal nanorods. J Nanosci Nanotechnol. **10**(2): 994-1000 (2010)

[24] Hui Zhang, Deren Yang, Xiangyang Ma, Yujie Ji, Jin Xu and Duanlin Que. Synthesis of flower-like ZnO nanostructures by an organic-free hydrothermal process. *Nanotechnology* **15** (5) 622 (2004)

[25] S.Chakraborty, A.K. Kole, P.Kumbhakar. Room temperature chemical synthesis of flower-like ZnO nanostructures. Mater. Lett. **67**, 362-364 (2012)

[26] Maryam Movahedi, Elaheh Kowsari, Ali R. Mahjoub, Issa Yavari. A task specific basic ionic liquid for synthesis of flower-like ZnO by hydrothermal method. Mater. Lett. **62** (23). 3856-3858 (2008)

[27] Xiaoju Luo, Zheng Lou, Lili Wang, Xuejun Zheng and Tong Zhang. Fabrication of flower-like ZnO nanosheet and nanorod-assembled hierarchical structures and their enhanced performance in gas sensors. *New J. Chem*, **38**, 84-89 (2014)

[28] Deren Yang , Yujie Ji, Xiangyang Ma, Jin Xu and Duanlin Que. Low temperature synthesis of flower-like ZnO nanostructures by Cetyltrimethylammonium bromide-assisted hydrothermal process. *J. Phys. Chem. B*, 2004, **108** (13), pp 3955–3958

[29] Jiang L[1], Feng X, Zhai J, Jin M, Song Y, Zhu D. High-yield self-assembly of flower-like ZnO nanostructures. J Nanosci Nanotechnol. **6**(6):1830-1832 (2006)

[30] Tsai Jenn Kai, Shih Jun Hong, Wu Tian Chiuan, Meen Teen Hang. n-ZnO nanorods/p+-Si (111) heterojunction light emitting diodes. Nanoscale Res. Lett. **7**(1):664 (2012)